Low-Frequency Atmospheric Acoustic Energy Associated with Vortices Produced by Thunderstorms

A. J. BEDARD JR.

National Oceanic and Atmospheric Administration/Environmental Research Laboratories/Environmental Technology Laboratory, Boulder, Colorado

(Manuscript received 15 July 2002, in final form 9 July 2004)

ABSTRACT

An infrasonic observatory collocated with the Colorado State University CHILL radar during the summer of 1995 permitted unique comparisons between severe storm kinematics and detected acoustic energy at subaudible frequencies near 1 Hz. Radar observations of a velocity couplet aloft (evolving into a tornado) showed a circulation maximum descending for about 30 min while moving to the east. The detected infrasound followed the trend of these observations. A model of sound radiated from vortex systems predicts frequencies in the range observed. These data are interpreted in the context of past infrasonic observations. An ongoing study comparing regional tornado and funnel sightings with archived infrasonic data has identified over 100 cases to date where the infrasonic signals occurred at the time of, and from the direction of, the vortices. For some of these cases, the distances were greater than 100 km. The author and his associates continue to collect datasets to permit further evaluation of infrasonic detection methods.

1. Introduction

This paper reviews the background of past measurements of acoustic energy at audible and infrasonic frequencies from severe weather and tornadoes. Infrasonic frequencies (i.e., sound below 20 Hz) can travel for great distances without significant absorption. Whereas a 1 kHz signal will have 90% of its energy absorbed after traveling 7 km at sea level, for a 1-Hz signal this distance is 3000 km (Cook 1962). Background concerning the measurements provided by infrasonic observing systems is provided in the appendix and in section 2.

A recent observation using an infrasonic observatory collocated with a Doppler radar provided a unique dataset for comparing infrasonic measurements with well-observed storm kinematics. The sound direction and elevation angle followed the trend of the movement of the vortex circulation maximum as a function of time. Sufficient information was available to compare the acoustic spectra with that predicted by sound generation models, suggesting that the sound originated from vortex radial modes of vibration. Radial vortex vibration as a source of infrasound is discussed in more detail in a later section.

Often we have noted that, when a number of strong cells are present in the region of an infrasonic observatory, acoustic energy is radiated by only one of the cells. Also, past lower-frequency geoacoustic measurements noted a relationship with large hail. This inspired the study of two significant hail-producing storms, well documented by Doppler radar. No acoustic energy was detected from either of these storms, and no evidence of vortices occurred. This indicates that near infrasound is not a common feature of all severe weather.

2. Historical perspective

a. Audible sounds

Numerous reports have described audible sounds from tornadoes (e.g., Brooks 1951; Hazen 1890), but few have included actual measurements of these sounds. An exception is the analysis of acoustic spectra from three tornadoes reported by Arnold et al. (1976). They used audiotape recordings taken by citizens at ranges of 1/2 mile, 200–300 yards, and, in one case, directly beneath a tornado as it traveled over the recording site. The dominant acoustic power for all three storms occurred at frequencies below 200 Hz. The sounds observed were between 100 Hz and 2 kHz. They also attempted to identify the sources of sounds that occurred at higher frequencies. They concluded that a study of variations in both low-frequency and high-frequency (HF) sounds as a tornado approaches and recedes seems a most promising method of gaining in-

---

Corresponding author address: A. J. Bedard Jr., NOAA/ERL/Environmental Technology Laboratory, R/ET1, 325 Broadway, Boulder, CO 80305-3328.
E-mail: Alfred.J.Bedard@noaa.gov

sight about internal circulations. They also noted the desirability of making measurements with arrays of microphones. However, because of the strong atmospheric attenuation at higher audible frequencies and the influence of wind noise, such measurements will be most useful relatively close to the vortex.

b. Atmospheric infrasound

Bedard and Georges (2000) provide background on measurements of atmospheric infrasound. In the past, using arrays of sensors designed to detect sounds at frequencies less than about 0.5 Hz, investigators measured infrasound originating from regions of severe weather. In some instances (e.g., Bowman and Bedard 1971), these detections were made at distances of over 1000 km from the source. Severe weather infrasound was investigated in a series of papers (e.g., Georges 1973, 1976; Beasley et al. 1976; Jones and Georges 1976) that compared the measured characteristics of the infrasound with a variety of potential sound generation mechanisms, considering a range of possible sources including release of latent heat, dipole radiators, turbulence, lightning, electrostatic sources, and vortex sound. In a comprehensive comparative study, Georges (1976) eliminated many sources as likely candidates and concluded that vortex sound was the most likely model. Georges and Greene (1975) noted that infrasound often precedes an observed tornado by up to an hour. In retrospect, it seems unlikely that the much lower frequencies detected by these geoacoustic observatories had any direct connection with tornado formation. Georges (1976) recommended that direct comparisons be made between infrasonic and Doppler radar measurements. However, at that time the sound generation process (or processes) had not been verified and low-frequency sound investigations were not continued, in part because of funding issues.

Other types of pressure wave disturbances radiate or are predicted to radiate from severe weather. These include atmospheric gravity waves (Bowman and Bedard 1971) and thermal acoustic waves (Nicholls et al. 1991). These much lower frequency pressure disturbances (having periods of tens of minutes) are not the focus of this paper. Thermal acoustic waves are predicted from the energy release of growing thunderstorms and propagate at acoustic velocities in the form of Lamb waves with horizontal particle motions (Gossard and Hooke 1975). These as well as atmospheric gravity waves could be valuable indicators of storm processes. For example, Bowman and Bedard (1971) have measured the propagation of atmospheric gravity waves over distances of hundreds of kilometers and suggested that arrays of pressure sensors can be used to predict arrival times at distant locations. Nichols et al. (1991) in numerical simulations found that thermal acoustic waves provide an index of storm energy release.

c. Near infrasound

Most past observations used acoustic passbands much lower in frequency than the 0.5- to 5-Hz frequency range focused on in this paper. Differences between the infrasonic measurement systems applied in the 1970s and 1980s as a part of a global observing network and the higher-frequency near-infrasound system detecting signals from a tornadic system on 7 June 1995 are significant. Several features of the global observing system (including the array dimensions, the spatial filter, and the sensor itself) combined to limit the high-frequency response to below 0.5 Hz. The severe-weather-related infrasound reported in the literature from the global infrasonic network involves sound two orders in magnitude longer in wavelength than the newer system and at continental scales of thousands of kilometers. In contrast, the near-infrasound system used to take the measurements reported here focuses on frequencies in the range 0.5 to 10 Hz and regional range scales of hundreds of kilometers or less. Table 1 summarizes the differences between these systems.

As an analog to the optical spectrum, the frequency range from about 1 to 20 Hz (just below the audible) is referred to as "near infrasound," as light just below the visible is called "near infrared." During the 1980s, as a component of a Department of Energy program to evaluate long-range acoustic detection capabilities, The National Oceanic and Atmospheric Administration's (NOAA) Wave Propagation Laboratory (WPL), now the Environmental Technology Laboratory (ETL), developed new hardware and software to monitor infrasound in a frequency range centered just above 1 Hz. This near-infrasonic system had quite different capabilities from the geoacoustic observatories operated prior to the mid-1980s as described above. As part of an ongoing effort to evaluate the near-infrasonic system, it was operated episodically to collect data on the types of signals occurring and to determine their origins. Since that time, it has detected signals related to a variety of sources including earthquakes, meteors, airflow over mountains, explosions, and avalanches, as well as severe weather. Bedard (1988) presented examples of

TABLE 1. Contrasting properties of the infrasound global network and current near-infrasound observing systems.

System	Typical sensor spacings	Spatial filter type	Typical acoustic wavelengths	Maximum HF response
Global infrasound observing system	10 km	1000 ft linear	3 to 30 km	0.5 Hz
Near-infrasound observing system	100 m	50 ft in diameter	30 to 300 m	>20 Hz

some of these sources. Balachandran (1979) and Bohannon et al. (1977) also reported infrasound from severe weather in this frequency range. The details of the severe weather systems radiating infrasound were not reported. They did not report infrasound originating from nonsevere weather.

A focus in this 0.5- to 2.5-Hz passband was on documenting severe-weather-related infrasound. Specifically, data were summarized during the summer months and the acoustic signals were compared with radar summary data. Bedard et al. (1986) provided some statistics comparing the acoustic bearings with storm location bearings, finding excellent agreement (typically within several degrees). They also provided data on signal amplitude as a function of range. One important case study demonstrated that the sounds being detected did not originate from cloud-to-ground lightning strike locations, as documented by a spherics network. This is consistent with the fact that the dominant frequencies of thunder measured by Few (1979) occurred at higher frequencies. Following on the work of Few, several researchers confirmed that the acoustic spectral peaks are in the audible range. For example, Bass (1980) in a theoretical and experimental study found that a typical spectral peak at longer ranges is near 100 Hz. Depasse (1994) made measurements of the dominant frequencies for lightning discharges at various distances, finding spectral peaks between 205 to 1715 Hz.

Beasley et al. (1976) searched for a relationship between infrasound detected from severe weather and lightning, concluding that infrasound is not caused by lightning. However, at near-infrasonic frequencies we continue to search for acoustic source mechanisms involving electrical activity. There still remains a possible alternative electrostatic generation mechanism, as suggested by Dessler (1973).

NOAA's National Hourly Radar Summaries were quite valuable for making comparisons with acoustic signals. The observation of 27 July 1985 (Fig. 1) is an example of long-range detection of infrasound associated with severe weather. In this case, the infrasonic observatory detected energy from a cell in Minnesota, 1000 km distant. Typically the infrasound recorded is from specific cells, but at such long ranges it is not possible to identify the particular storm features at the origin of the sound. At times the signal amplitudes were small, causing low signal-to-noise ratios and reduced azimuth resolution in processing. This degradation could cause a sector of azimuths to be displayed (typically +/−5°). The center of the sector usually corresponded to the storm locations to within 1°–2°. At shorter ranges of 100–200 km or less, usually sharp, discrete azimuths were obtained with sector widths often 1°–2°.

Figure 2 is an example of a nearby detection on 23 July 1985, showing a shift of azimuth with time. The upper panel shows higher correlation values of azimuth from which infrasound was detected. This example was chosen to illustrate the ability of infrasonic observatories to monitor direction changes. For good quality signals, the direction of arrival can be estimated to about 1°. The clearest persistent signal initially comes from the southeast at 150° and then shifts to a second persistent direction from about 130°. The trend is for a shift from 170° to 120° over about a half hour. The lower panel is the dominant frequency for each processing interval, indicating an increase in frequency cor-

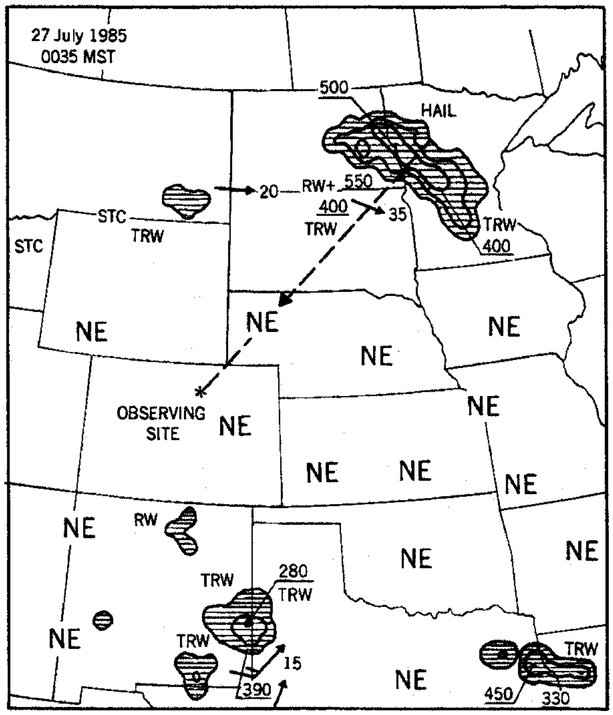

FIG. 1. Detection of infrasound on 27 Jul 1985 from severe weather located about 1000 km away from the observatory. The dashed line indicates the azimuth of the infrasonic signal detected. NE indicates no echoes.

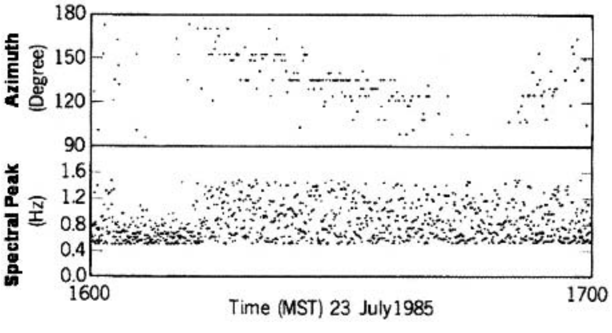

FIG. 2. Detection of infrasound from nearby severe weather showing shifts in azimuth as a function of time and an increase in the dominant frequency measured, limited to processed data showing only higher signal-to-noise ratios (measured as cross-correlation coefficients as indicated in section 4b) and show the azimuth values from which sound was detected and the associated dominant frequencies.

responding to the start of the higher correlation and azimuth shifts. Although relatively smooth, progressive changes in direction are observed; often for nearby signals associated with severe weather such discrete changes in direction are observed. Such discrete changes could result from new source regions developing within a storm or from variability of atmospheric wind speed or temperature gradients along propagation paths.

Data for the summer of 1985 were summarized by dominant storm features in Fig. 3. These signal characterizations were based upon radar summary data, so no detailed knowledge of the storm's internal dynamics was available. Practically all of the storms generating infrasound could be classified as significant in that they produced hail, had tops of >45 000 ft, or created a hook echo. During the spring and summer months in Colorado and nearby regions there are no other sources of infrasound having the characteristics of those associated with severe weather. Rather the evidence to date is that sources of potential false alarms could be signals originating from nontornadic storm processes.

Figure 4 summarizes data on the amplitude of detected acoustic waves as a function of distance to the storm, together with inverse distance and the square root of inverse distance lines. The expected decay of sound pressure level from geometrical spreading with distance is inversely with range. However, the atmospheric temperature and wind structure trap much of the acoustic energy, producing a waveguide (Georges and Beasley 1977). Thus, if we assume that the sound generation pressures are approximately the same for the various sources, an inverse square root of the distance is a better fit to these data. This rough pressure–amplitude range relationship permits us to make estimates of detection threshold at various distances. Most distant storms have pressure amplitudes from 0.01 to 0.1 Pa (peak to peak), which are easily detected under normal conditions.

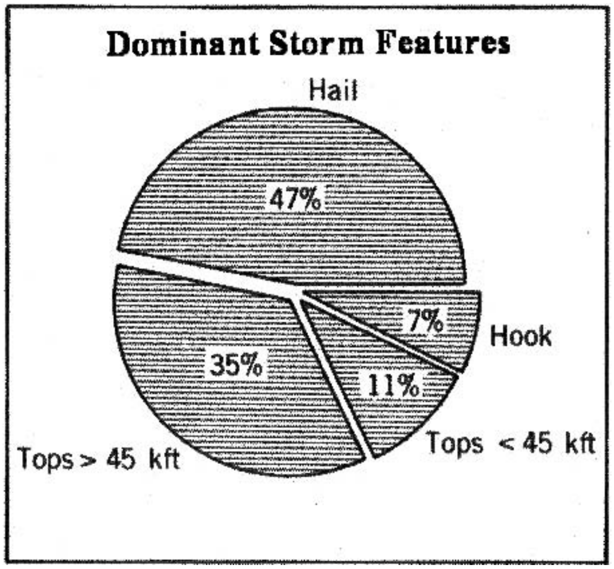

FIG. 3. Distribution of dominant storm features associated with infrasound as derived from hourly radar summaries.

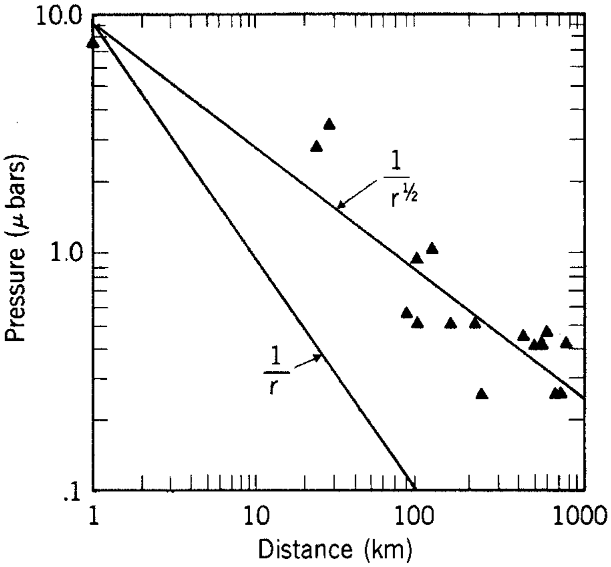

FIG. 4. Peak-to-peak amplitude of measured infrasound as a function of distance from severe weather sources.

Bedard et al. (1988) also presented evidence that avalanches radiated infrasound that could be detected at distances of hundreds of kilometers. In 1993, an evaluation program was started, and during the winter of 1993/94, a system was installed at a location near numerous avalanche paths. Bedard (1994) summarized results showing the clear detection of avalanches, and work began on creating a practical, multi-observatory monitoring system. A system located in Colorado near Red Mountain Pass during the winter of 1994/95 provided more detections, but it was clear that two systems working together would be necessary to pinpoint locations. Thus, we set about to develop the data transfer and multistation analysis capability for an avalanche system, working during the summer months of 1995. This set the stage for the measurements described in this paper.

Another factor was the prediction by Nicholls et al. (1991) of the severe weather generation of thermal acoustic waves, and a system was planned for their detection (Pielke et al. 1993). The plan for the detection of thermal acoustic waves included three mobile single-pressure-sensor observing systems to be located under the direction of a Doppler radar. Therefore, it seemed logical to place one of the two near-infrasound observatories at the site of the Doppler radar to monitor severe weather and exercise the avalanche detection system.

3. Instrumentation overview

Each infrasonic detection system consists of an array of four sensors in a roughly square configuration about

100 m on a side. Because of the need to reduce the pressure noise from atmospheric turbulence and other sources, each sensor is connected to a device that filters out subscale spatial noise. The long-wavelength infrasonic signals are not affected by this filter. The theory of operation of these noise-reducing devices is described by Bedard (1977). Over the years, changes have made the filters more effective, but the basic principle of operation has remained essentially the same. Cook and Bedard (1971) described a typical infrasonic system design. Processing was performed by cross correlating data from the various sensors to define the azimuth, searching for coherent energy propagating at acoustic or higher phase speeds. Processing details are provided by Einaudi et al. (1989). The appendix provides more information on the parameters that are measured.

In the early 1970s and before, processing was performed using an analog correlator. This was replaced by a large dedicated computer, and processing was done after the fact. Data are now processed and archived using two desktop computers: one is dedicated to acquisition and archiving, the other to beamsteer processing of data blocks and archiving of the processed data. A global positioning system receiver is used to synchronize and maintain accurate time. Modems are used to maintain telephone contact with a central computer at a remote site. Calls are made automatically from the central site at preset times, and the observatory computer is programmed to listen for these incoming calls. Every few days, the data are downloaded from the observatory computer to tape. Under development is the capability to ingest data from two observatories and display the acoustic bearings and azimuth intersections in essentially real time. During the summer of 1995, one observatory operated to the east of Boulder, Colorado, at the Boulder Atmospheric Observatory (BAO), and the other operated at the Colorado State University (CSU)–CHILL[1] radar site in Greeley, Colorado.

The CHILL radar is an 11-cm-wavelength Doppler radar used with an 8.5-m-diameter parabolic antenna, providing a 1.1° half-power beamwidth. Range gates from 15 to 150 m are available. Several real-time display options make the system ideal for guiding field operations. Datasets from the CHILL radar and infrasonic observatory are compared in the next section.

4. Observations of the evolution of vortices

a. Doppler radar observations

On 7 June 1995, the CSU–CHILL Doppler radar tracked a storm system moving from southwest to northeast. Cary and Rutledge (1998) made hail, lightning, and radar comparisons for this storm following the evolution from 1731 to 2028 mountain daylight time (MDT). During the period 1847 to 1916 MDT, Cary and Rutledge list three public reports of large hail and a tornado. They describe the tornado, sighted at 1924 MDT, as appearing to occur on a descending hail curtain adjacent to the storm updraft. Hubbert et al. (1998) described the synoptic-scale environment of this system. Hubbert et al. (1998) focused on the storm microphysics from 1720 until about 1835 MDT. They characterized the storm as a High Plains supercell storm. They tracked the storm motion from 1720 until 1850 MDT, about the time when the storm was south of the CHILL radar and infrasound was first clearly detected. Early in the sequence of scans (starting about 1900 MDT), several cyclonic radial-velocity couplets occurred along a flanking line. Shortly, these small couplets seemed to be amalgamated into an evolving, larger-scale circulation. The volume scans were analyzed between 1850 and 1929 MDT, and the radar elevation angle containing the strongest circulations in each volume scan was identified. Some of the scans showed clear radial-velocity couplets, while for others it was more difficult to identify the vortices, suggesting the circulation was weakly organized. In spite of this, two vortices could be tracked. Vortex 1, at a range of about 14 km, could be identified from 1850 to 1924 MDT. The largest values of circulation were seen first at higher elevations and later at lower elevations. At 1924 MDT, the region of maximum circulation was near the surface, and a tornado was sighted. The cyclonic rotation couplet moved to the east throughout this interval. At 1929 MDT, the couplet was no longer evident. Figures 5 through 8 show reflectivity and radial-velocity images at 1901 and 1924 MDT.

Near 1924 MDT tornado sightings were reported to the National Weather Service (NWS) from the region of Kersey, Colorado (which is at an azimuth of 138° and a range of 7.6 km from the radar). The locations of the two most persistent vortices are plotted on a map of the area as a function of time (Fig. 9). The sequence of radar observations provided a picture of the evolution and interplay between various scales of vortices and will be a fruitful dataset for future study. The focus here, however, is to compare the radar documentation of intensity and radial velocity with infrasound detected during the same time interval. Thus, we address defining the characteristics of the circulations as a function of time to help identify any acoustic source generation mechanisms present. Estimates were made of the vortex azimuth, range, and elevation angle to the circulation maximum. In addition, estimates made of the circulation outside the vortex core (which is a measure of the total angular momentum of the system), the core diameter, and the average maximum tangential speed are plotted together in Fig. 10. Since the values for

---

[1] Historically, the radar was operated by both the University of Chicago and the University of Illinois; hence, the origin of the name CHILL.

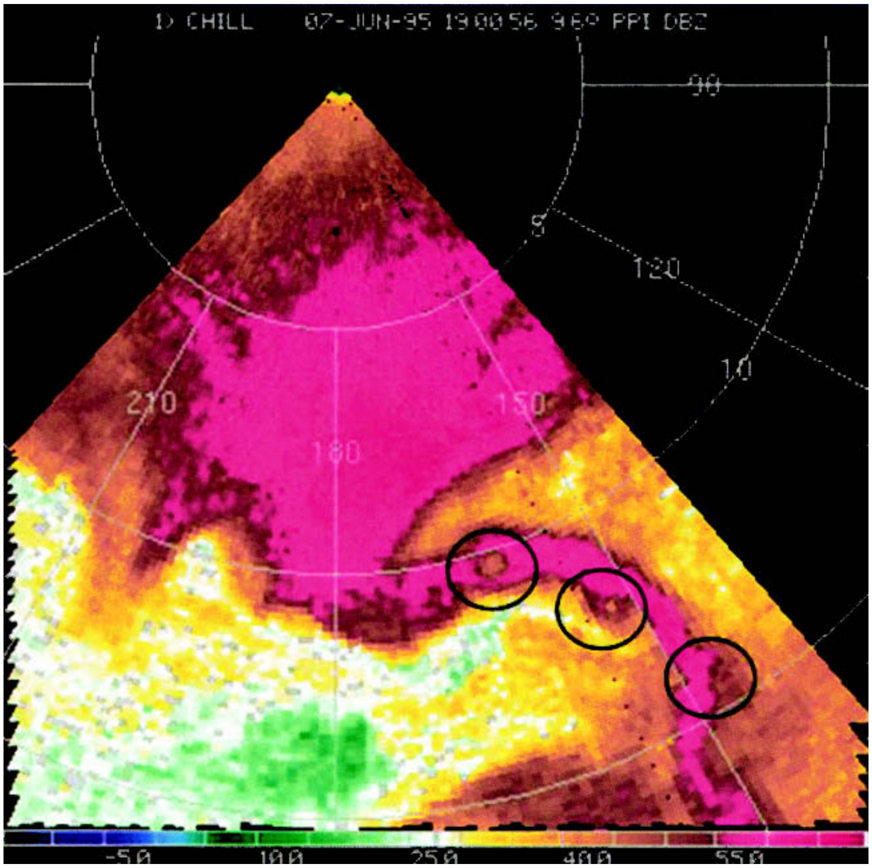

FIG. 5. 1901 MDT on 7 Jun 1995: reflectivity (dBZ); elevation angle, 9.6°; range rings are 5 km. The circles indicate the locations of reflectivity eyes (regions of low reflectivity indicating vortex cores).

tangential speed and radius inferred from radar remain approximately constant throughout the interval, the circulation that is proportional to their product outside the core region also remains constant.

b. Infrasonic observations

This section reviews the acoustic signals that occurred on 7 June 1995 between about 1850 and 1924 MDT at the Greeley Observatory. Figure 11 shows plots of correlation coefficient and azimuth as a function of time, covering the interval of the radar observations. The interval shown is from 1555 to 2155 MDT to emphasize that the feature that appears from 1850 to 1924 MDT differs from the background, appearing as a well-defined increase and decrease of signal quality. Subsequent figures show this interval in more detail.

The correlation coefficient is a critical index for identifying signals in a quantitative way. We measure the cross correlation between sensor outputs as relative time delays consistent with the passage of plane wave fronts across the array elements. With a measuring network of N sensors and R_{ij} the cross-correlation coefficient between two pressure signals from sensors i and j, the average correlation coefficient R_{ave} is

$$R_{\mathrm{ave}} = \frac{2}{N(N-1)} \sum_{i=1}^{N-1} \sum_{j=i+1}^{N} R_{ij}. \tag{1}$$

The signal-to-noise ratio, S/N, is related to R_{ave} by the expression

$$\mathrm{S/N} = R_{\mathrm{ave}}/(1 - R_{\mathrm{ave}}). \tag{2}$$

For $R_{\mathrm{ave}} = 0.5$, the S/N is 1 and such signals can usually be easily identified. At $R_{\mathrm{ave}} = 1$ the S/N is infinite and often we have high quality signals approaching this value. For a persistent low-level signal we can often identify signals with values of R_{ave} near 0.3 or a S/N value of about 0.4. As an example, an infrasonic signal level of 0.1 Pa at S/N of 0.4 would correspond to boundary layer eddy noise of 0.25 Pa. Measurements of wind-induced pressure fluctuations in the 0.5- to 5-Hz passband indicate that without the use of spatial filters, pressure fluctuations of this magnitude would correspond to a wind speed of about 7 m s^{-1} under most conditions (Bedard et al. 1992). The use of spatial filters

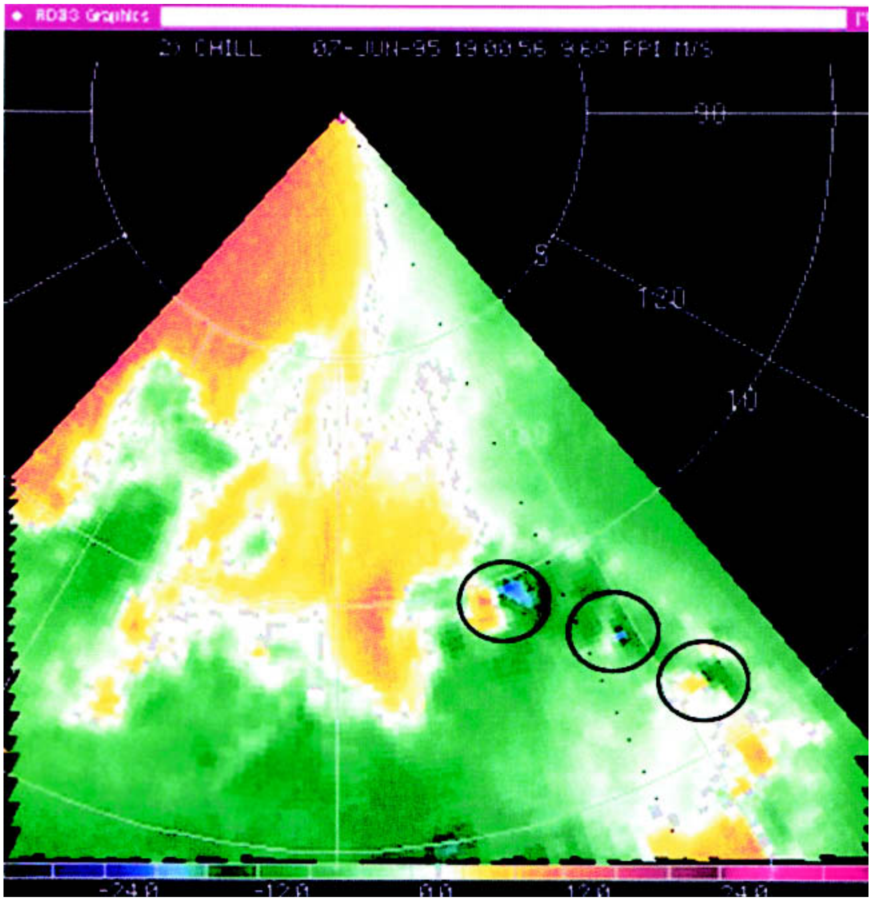

FIG. 6. 1901 MDT on 7 Jun 1995: radial velocity (m s^{-1}); elevation angle, 9.6°; range rings are 5 km. The circles indicate the locations of velocity couplets.

can reduce this form of noise by an order of magnitude or more (Bedard 1977), enabling signal detection in the presence of winds in excess of 20 m s^{-1}. An improved understanding of boundary layer turbulent pressure fluctuations will certainly lead to improvements in wind-noise reduction and measurement site selection.

Note that during the period of interest, a region of higher correlation coefficients corresponds to azimuths changing from southeast to east-southeast. Many infrasonic signals from severe weather have high persistent correlation coefficients (often in excess of 0.7). The signal shown in Fig. 11 is of weaker quality. However, the correlation values monotonically increase and decrease above the noise floor, corresponding to an interval of progressive azimuth shift. These data for the critical period were then reprocessed, with only time blocks with correlation coefficients greater than 0.4 displayed in Fig. 12. The signal does appear at correlation coefficients less than 0.4 for a longer period of time until 1924 MDT, but Fig. 12 shows the trend more clearly by removing noise. A clear trend of azimuth shift with time is evident, with the direction from which signals are arriving shifting from about 160° near 1900 MDT to 100° near 1924 MDT, following the trends of the variation of the velocity couplet radar azimuth with time. A puzzling aspect of this observation is that the radar bearings to the dominant vortex superimposed on the plot are consistently more southerly by 10° to 40°. A possible explanation involving refraction effects by horizontal wind gradients is discussed in a following section. It is certainly possible that another storm feature exists traveling along with and near the vortex. Another interesting feature of the infrasonic observations is illustrated in Fig. 13, a plot of horizontal phase speed and dominant frequency as a function of time. The infrasonic system measures the acoustic phase speed, C_p, directly using the time that it takes a wave front to traverse the array of sensors. This can be interpreted in terms of an elevation angle. Where C is the local sound speed, $C_p = C$ indicates that the wave is propagating horizontally at the local speed of sound. For waves incident from directly overhead, C_p is infinite. For intermediate elevation angles, $C_p = C/\cos\alpha$, where α is the elevation angle relative to the surface of the earth. An acoustic phase speed of about 330 m s^{-1} indicates that the sound wave is moving across the array

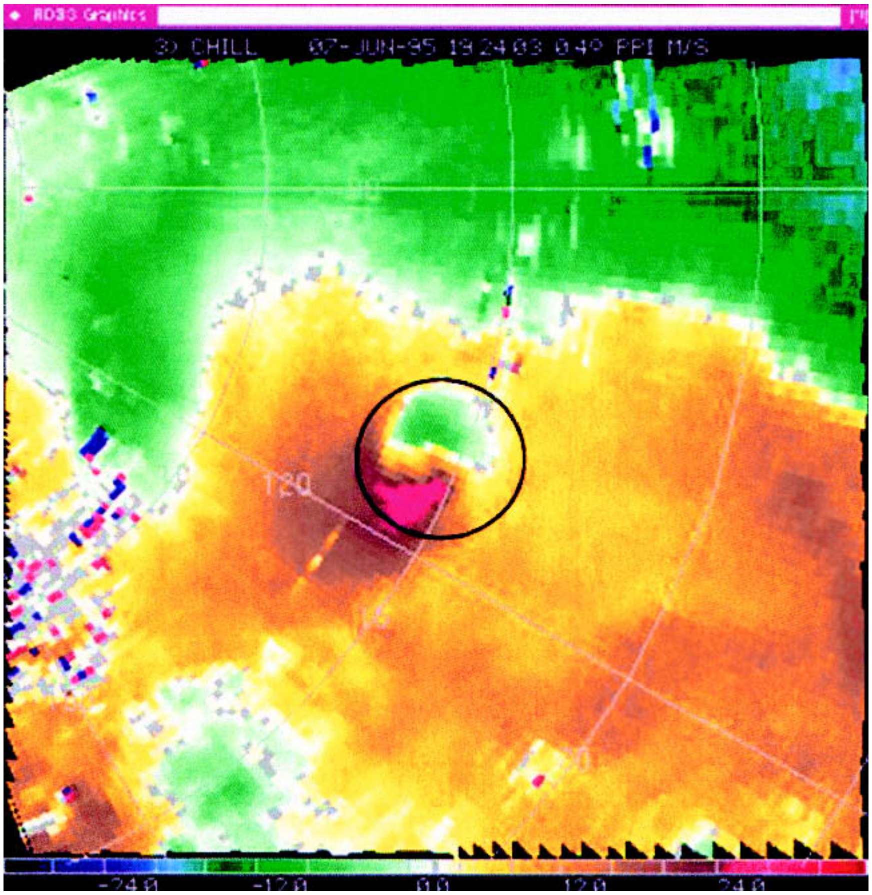

FIG. 7. 1924 MDT on 7 Jun 1995: radial velocity (m s^{-1}); elevation angle, 0.4°; range rings are 5 km. The circle indicates the location of the velocity couplet.

horizontal to the surface of the earth, at a 0° elevation angle. If phase speeds higher than the local speed of sound are recorded, one likely explanation is that the sound is arriving from above, at some angle to the surface of the earth. An alternative explanation is that the measured pressure waves are locally coupled from seismic waves, which propagate at about 10 times the speed of sound in air (Bedard 1971). Measurements of infrasound having high phase speeds shifting with time are often related to meteors (Bedard and Greene 1981). However, meteor infrasonic signals are usually less than a minute in duration, showing quite rapid shifts in phase speed and azimuth. In this case, the waves arrived near 1900 MDT at speeds of about 700 m s^{-1}, decreasing to the local speed of sound near 1924 MDT, indicating an initial source region aloft that moved slowly down to the surface of the earth.

The dominant frequency was the spectral peak in a passband from 0.5 to 2.5 Hz. The processing was done over the entire frequency range of 0.5 to 2.5 Hz, but the processing algorithm only picks out the dominant frequency for display. The dataset was processed over a range of passbands, but the 0.5- to 2.5-Hz passband best represented the signals detected (having the highest correlation coefficient). Most of the peak frequencies occurred between 0.5 and 1 Hz, with a trend for some sporadic data at higher frequencies (near 1.5 Hz) to occur midway through the time interval. Figure 14 presents infrasonic time series for two of the array microphone channels. The waveforms are similar for the two channels, indicating a coherent wave moving across the array at least at the speed of sound. The other two channel time series are essentially identical in waveform, only shifted slightly with time. The amplitude is about 1 Pa (peak to peak). Such signals could be detected at ranges of hundreds of kilometers from a source for typical acoustic propagation conditions.

c. Comparisons of radar and acoustic measurements

It was observed (Fig. 12) that both the radar azimuths for the location of the circulation and the acoustic azimuths showed similar trends, indicating a source moving from the southeast to the east-southeast over the same half-hour interval. There is a small delay time for

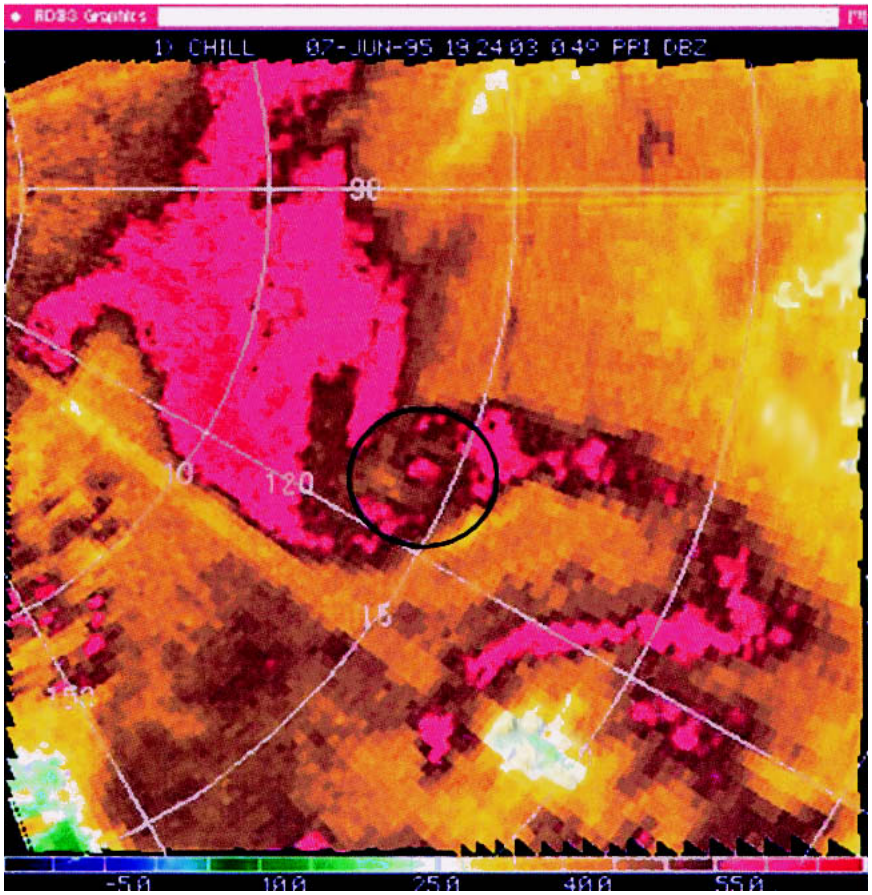

FIG. 8. 1924 MDT on 7 Jun 1995: reflectivity (dBZ); elevation angle, 0.4°; range rings are 5 km. The circle indicates the location of the velocity couplet.

sound propagation, but at ranges of 10 km this is only about 30 s.

Similarly, it was observed that the elevation angle for the maximum vortex circulation descended to near the surface from initial values of about 20°. The angle corresponding to the acoustic measurements is computed and plotted together with the radar angle in Fig. 15. The acoustic energy was apparently originating higher in the system for the first 15 min than the velocity couplet maximum indicated by the radar. If the sound source was, in fact, related to the circulation, higher-angle radar scans may not have detected significant radial velocity components initially because of the orientation of the vortex relative to the radar beam. During the last 15 min, there was good agreement between the angle-of-descent measurements with time for the two systems.

d. Estimates of wind shear–induced bearing errors

The consistent difference between the infrasonic bearings and the radar bearings requires more examination. These differences are emphasized by the composite view in Fig. 16, showing the infrasonic bearing sectors relative to the vortex location at 1903 and 1924 MDT. In spite of the fact that elevation angle and bearing trends track, the radar bearings to the vortex are more southerly by 10° to 40°. The array geometries used in the infrasound involve sensor separations of about 100 m that routinely provide bearing accuracies to 1°. The most likely causes of the disagreement are either that another source was being detected or that refraction effects were responsible for bearing deviations. The vortex descending from aloft was embedded in a larger-scale mesocyclone circulation creating horizontal wind speed gradients. There was no other storm feature that followed the bearing and elevation angle trends. There was also a second vortex at closer ranges detected for some of the interval along similar radar bearings. Early in the period, this second vortex created horizontal wind speed gradients almost directly along the expected acoustic bearing from the first vortex to the infrasonic observatory at the radar site. Thus, there are two possible explanations for acoustic bearing errors. One mechanism is that the intermediate vortex disrupted the direct-sound ray path with complex focusing and defocusing (e.g., Georges 1972). However,

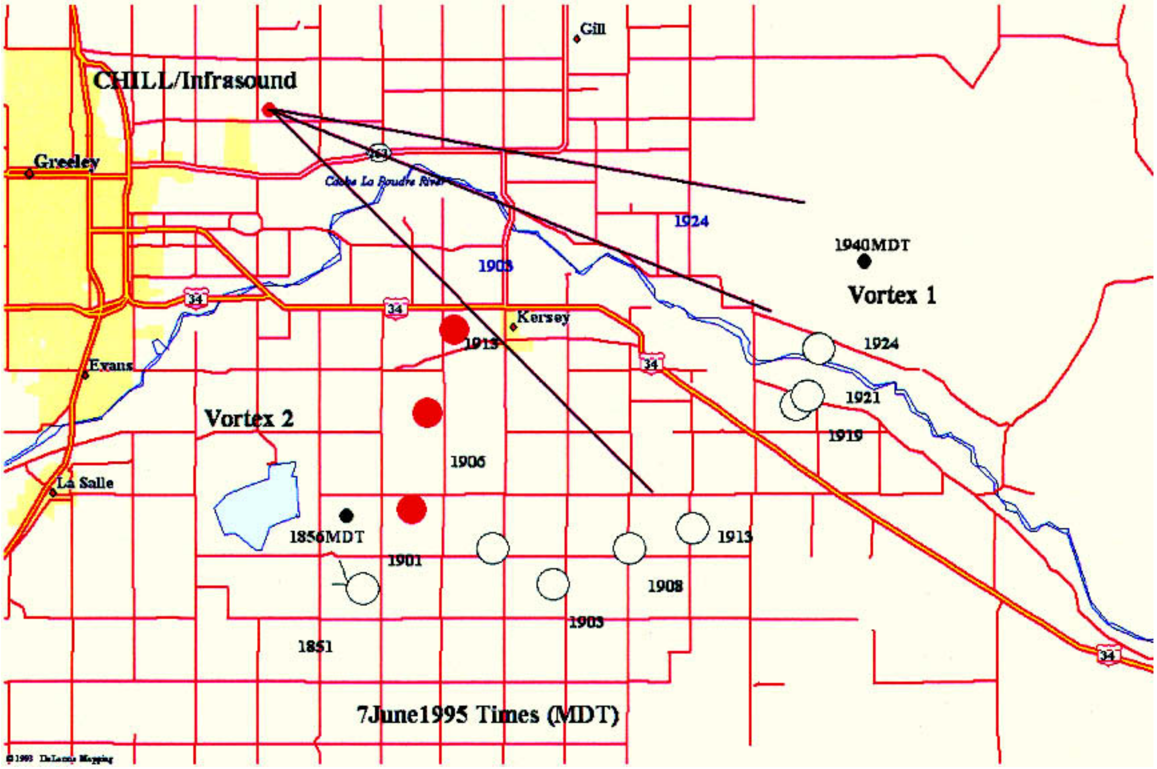

FIG. 9. Locations of two vortices determined by Doppler radar on 7 Jun 1995. Vortex 1 (white circles) and vortex 2 (red circles) are indicated on the base map for a series of MDT times. Two measured infrasonic azimuth sectors are plotted at 1903 and 1924 MDT. Locations of observed tornadoes from *Storm Data* are indicated by the smaller black circles at 1856 and 1940 MDT. There were additional chase team and observer reports during the period, including one near 1924 UTC.

this vortex was not detected during the later portion of the period. Another possibility is that the segment of mesocyclone circulation just to the north of the vortex refracted the acoustic ray paths. Because the vortex moved with the mesocyclone there was a strong horizontal wind speed gradient (e.g., 20 m s^{-1} over several kilometers) present throughout the time of these observations. Performing ray trace calculations for a horizontal wind speed gradient of 20 m s^{-1} over 2 km indicated that bearing deviations in the range of 10° to 40° could easily occur under these conditions. Because of the complex three-dimensional structure of the wind field surrounding the vortex it is possible that some focusing of sound also was taking place, making the easterly infrasonic bearings more dominant than direct ray paths. This case indicates the importance of horizontal gradients and the need to model a variety of situations using three-dimensional ray trace simulations. Figure 17 is a radar image for an intermediate scan at 1913 MDT when the circulations are not as evident. The locations of circulations are indicated by circles. The radial velocity toward the radar is to the north, and possible refracted ray paths are indicated.

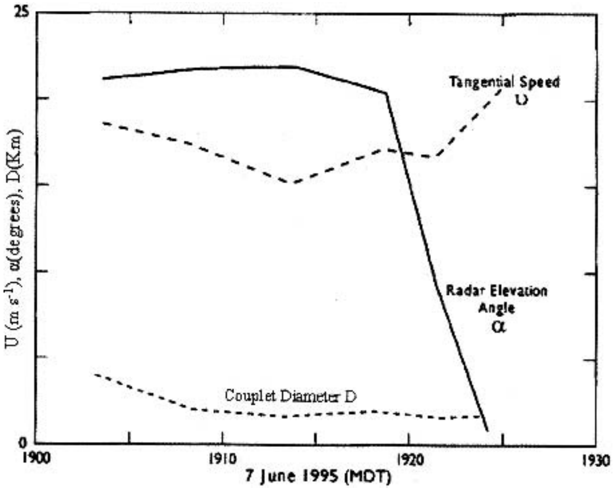

FIG. 10. Radar estimates of elevation angle, couplet diameter, and tangential speed of the vortex maximum throughout its lifetime.

e. Bearing errors and travel time delays

Past measurements made from infrasound from weather and other geophysical events used instrumentation that responded to frequencies below 0.5 Hz. In addition, the array spacings were typically 5 to 10 km

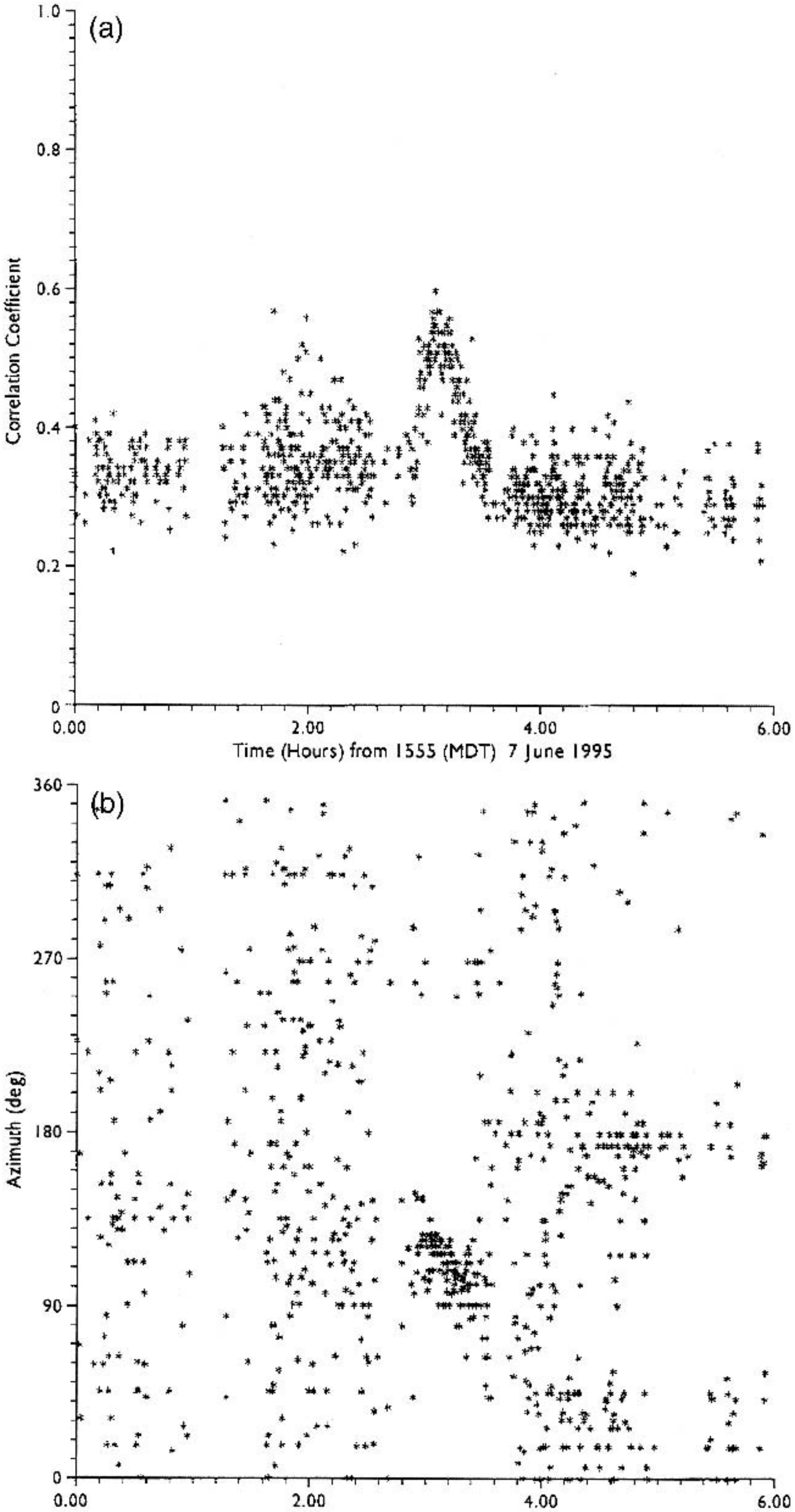

FIG. 11. Infrasonic (a) correlation coefficient and (b) azimuth as a function of time for all values of the correlation coefficient.

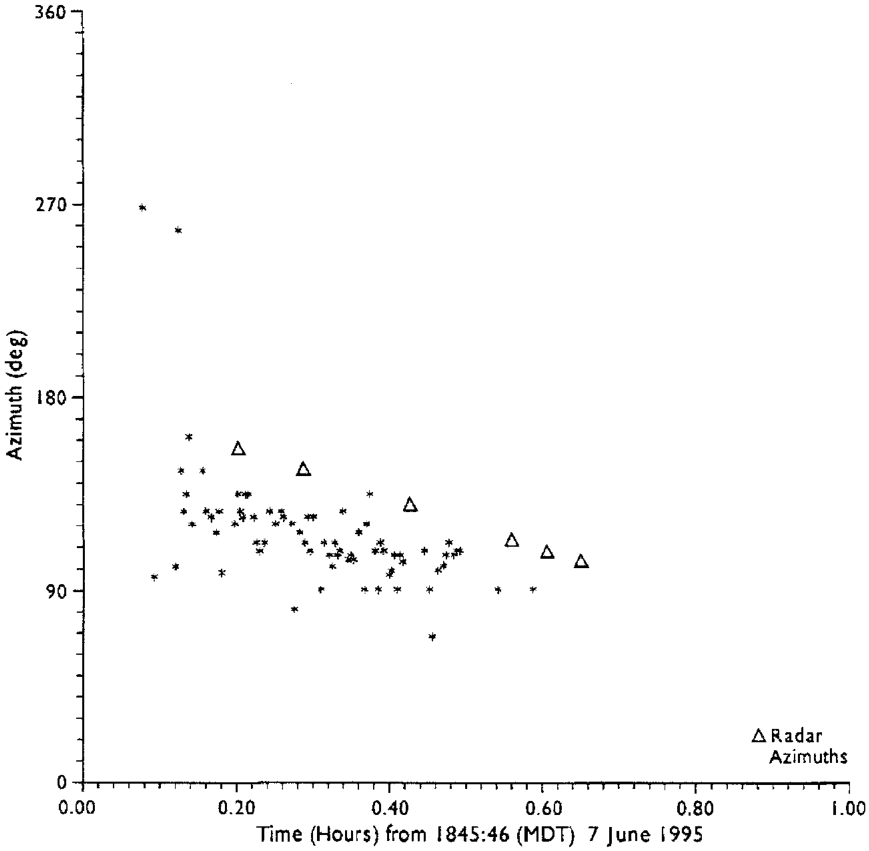

FIG. 12. Infrasonic azimuth as a function of time for data with correlation coefficients greater than 0.4. The triangular points on the azimuth plot are the radar bearings to the vortex.

because frequencies less than 0.1 Hz were of primary interest. Most of our early knowledge about propagation and signal characteristics involved these lower frequencies, and typical ranges were at continental scales. Usually global arrays of geoacoustic observatories detected signals after long propagation paths and atmospheric temperature and wind structure had important effects on the measured waveforms, travel times, and bearings. Georges and Beasley (1977) computed the effects of wind refraction on such long-distance paths (1000 km). Most pertinent to the measurements reported here are the summer mean wind model results of Georges and Beasley (1977) for midlatitudes, which show quite small bearing deviations (usually less than 1°).

On the other hand, the effects of smaller-scale near-storm-environment wind and temperature structures have not been well investigated. We are currently starting to apply an acoustic ray trace program to systematically evaluate the effects of storm environment wind and temperature gradients on measured bearings. If sound radiation comes from sources on smaller scales than the storm system in which it is embedded, there is the possibility that nearby larger-scale wind speed and temperature gradients (e.g., from outflows or inflows) will refract sound rays, causing bearing errors, focusing, and defocusing. Georges (1972) computed the ray paths for sound waves traversing a vortex showing the important effects that can occur. If such refraction becomes important we would expect to detect large, chaotic, and rapid bearing and elevation angle deviations. A typical detection associated with a tornado shows a well-defined azimuth that progressively tracks the storm with time. Our experiences of usually detecting accurate bearings could be because vortices extended vertically and radiating sound along the length of their cores create numerous ray paths. Only a subset of these rays may encounter strong refraction effects. However, bearing errors and their sources should continue to be documented, and the case study presented here probably represents an example of important refraction effects. Our experiences with the detections of known regional sources of sound (e.g., sporadic ignited releases of combustible gas over an 8-month period at a range of 12 km) show accurate bearings to about 1°, and such sources can be valuable in studying propagation effects.

In contrast with continental propagation paths, acoustic systems intended to provide tornado warnings need to be close enough to the source of sound so that

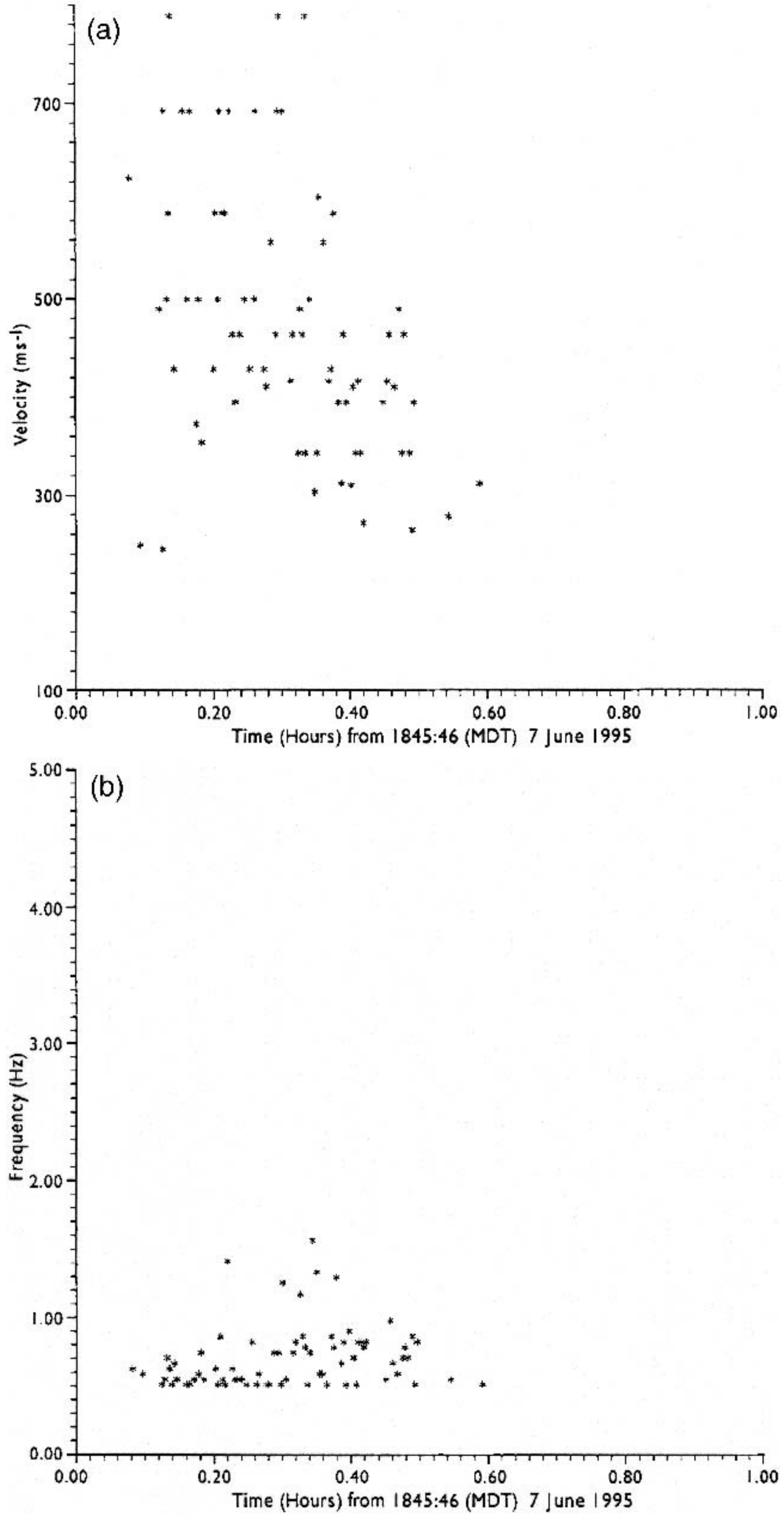

FIG. 13. Infrasonic (a) horizontal phase speed and (b) dominant frequency as a function of time.

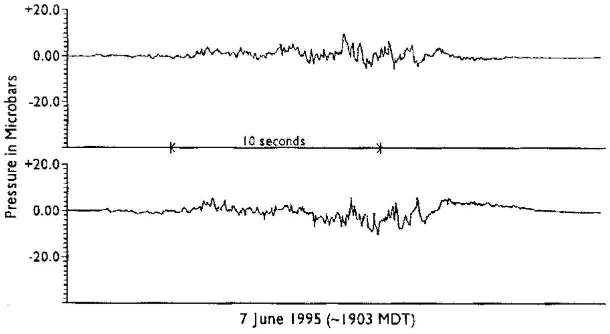

FIG. 14. Infrasonic time series for two of the array microphones.

the delays caused by acoustic propagation time do not remove any warning potential. Figure 18 is a plot of acoustic travel time in seconds as a function of distance in kilometers. At a range of 100 km there is a delay of about 5 min in detecting the sound [about the same as the time between Weather Surveillance Radar-1988 Doppler (WSR-88D) scan repetitions]. At longer range, our detection of a tornado occurring at Spenser, South Dakota, was delayed traveling a distance of 750 km by about 1 h (Bedard 1998). Such longer-range observations can be valuable for evaluating infrasonic systems or for research purposes. For example, after correcting for travel time, we found that the sound originated in the South Dakota region about 30 min prior to the tornado reaching Spenser. The impact of acoustic travel time delays are an important consideration in the design of infrasonic systems to provide warnings, and station separations in the range of 100 to 200 km are indicated.

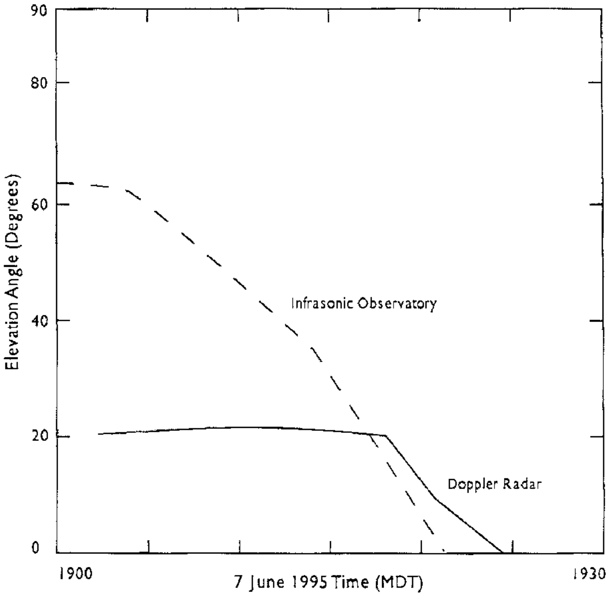

FIG. 15. Elevation angle of detected infrasound and radar elevation angle of the circulation maximum as a function of time.

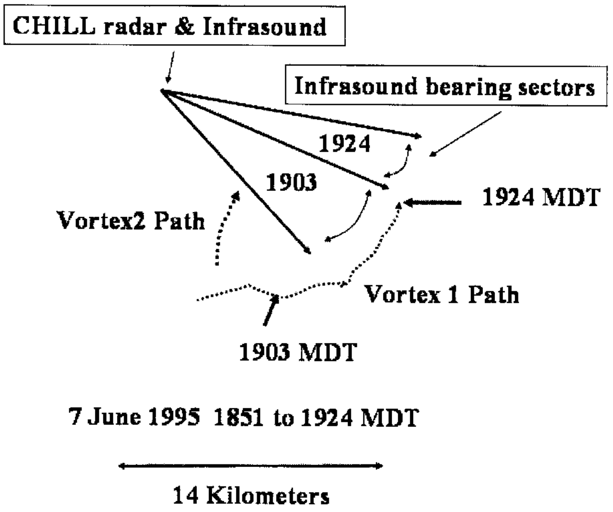

FIG. 16. Composite view showing the infrasonic bearing sectors relative to the vortex location at 1903 and 1924 MDT.

5. A comparison with sound generation models

a. *A review of possible sound generation mechanisms*

Because of the low-frequency content of large nuclear explosions (typically below about 0.2 Hz), the global monitoring systems were directed to this very low frequency passband. Conversely, the focus of other investigators was directed to the low audio (e.g., Few 1979). Many, but not all, of the past theories of processes capable of generating infrasound were directed toward frequencies either lower than 0.5 Hz or higher than 5 Hz; thus, they did not include our measurement passband. It is still useful to summarize the range of potential infrasound generation processes, since many of these theories could still describe other important aspects of severe weather physics. There have been a number of papers addressing aerodynamic sources of sound and vortex instabilities. Table 2 summarizes a number of these investigations, listing some key references for readers who are interested in these topics.

Many of the proposed sound-source mechanisms involve vortex sound production, either by radial vibration processes (e.g., Abdullah 1966) or flow instabilities (Georges 1976), and corotating multiple vortices (e.g., Mitchell et al. 1992). An additional process involves boundary layer pressure fluctuations (Tatom et al. 1995). Because a past study showed no correlations with cloud-to-ground lightning discharges in the 0.5- to 2.5-Hz frequency range, and because electrostatic processes (e.g., Dessler 1973) seemed unlikely to descend slowly to the surface, these electrical mechanisms are not considered further here. Any combination of the generation mechanisms mentioned above could be important at different frequencies.

Figure 19 is an example of the signal power spectra as

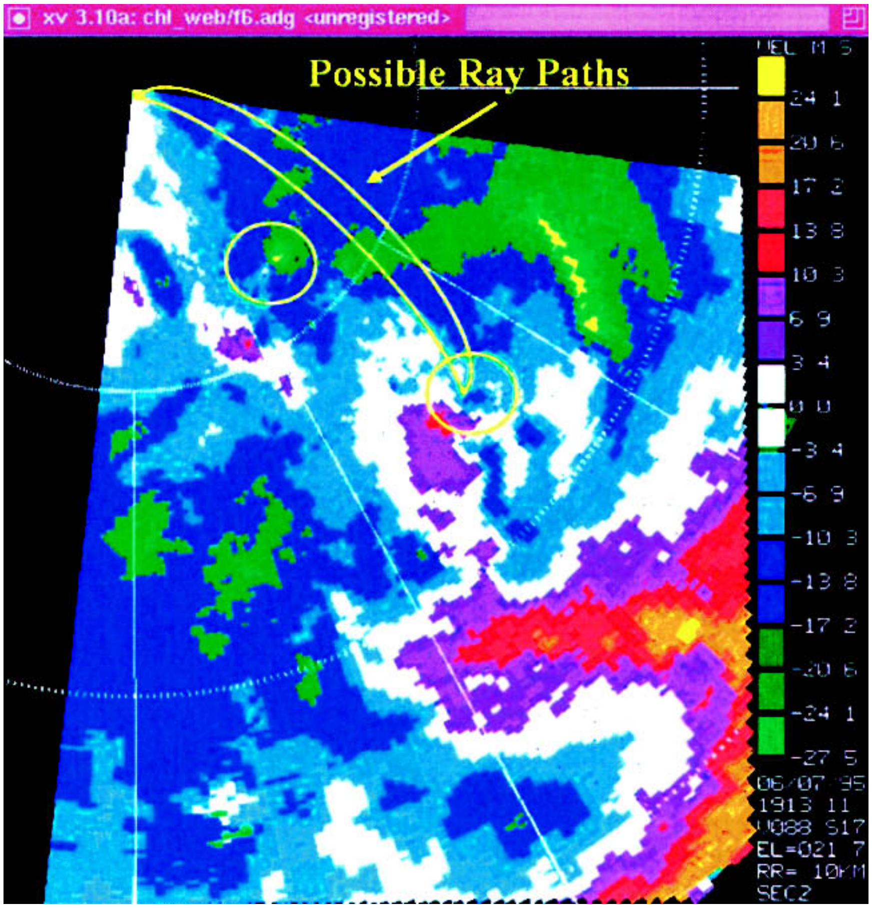
xv 3.10a: chl_web/f6.adg <unregistered>
Possible Ray Paths
VEL M S
24 1
20 6
17 2
13 8
10 3
6 9
3 4
0 0
-3 4
-6 9
-10 3
-13 8
-17 2
-20 6
-24 1
-27 5
06/07/95
1913 11
V088 S17
EL=021 7
RR= 10KM
SEC2

FIG. 17. Radial-velocity radar image with possible refracted ray paths indicated. 1913 MDT on 7 Jun 1995: elevation angle 21.7°; range rings are 10 km. The circles indicate the locations of velocity couplets.

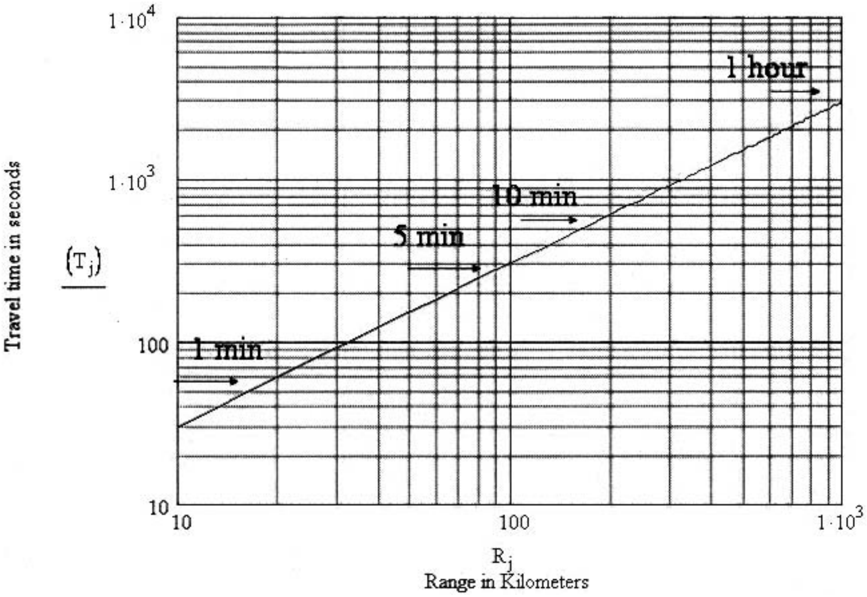

FIG. 18. Acoustic travel time as a function of range in kilometers.

TABLE 2. Theoretical investigations of potential severe weather sound generation processes.

Investigators	Physical process	Comments
Hicks (1884)	Vortex vibrations	Hollow core vortex
Thompson (1910)	Vortex vibrations	Realistic model
Lamb (1945)	Review of past work on vortex vibrations and waves	
Powell (1964)	Theory of vortex sound	
Anderson and Freier (1965)	Tornado wave motion	
Abdullah (1966)	Tornado radial mode vibrations as a sound source	Focused on audible detection
Colgate and McKee (1969)	Electrostatic sound	
Dessler (1973)	Electrostatic sound	
Meecham (1971)	Turbulence	
Georges (1976)	Comparative review of generation processes	Concluded vortex sound processes were most likely
Few (1979)	Lightning	
Lyamshev and Skvortsov (1988)	Review of vortex sound mechanisms	
Kozel et al. (1992)	Vortex wave effects	
Mitchell et al. (1992)	Sounds from corotating vortices	Numerical model showing evolution of the system
Tatom et al. (1995)	Seismic waves from tornado–surface interactions	Suggested the basis for a detection system

a function of time. Each time block processed is 12.8 s in duration with a Hanning window applied and overlapped in time. This plot covers about 6 min in time and shows a trend for higher frequencies early in the interval, with a dominant frequency near 0.5 Hz near the end.

b. *Infrasonic data compared with selected sound generation models*

Three sound generation models were chosen for comparison with the infrasonic data and are shown conceptually in Fig. 20. These models are the radial-modes-of-vibration model of Abdullah (1966), the tornado/boundary interaction model of Tatom et al. (1995), and the corotating vortex model (Powell 1964; Georges 1976; Mitchell et al. 1992). The infrasonic data seemed most consistent with the model of Abdullah, as is shown in a later section.

Abdullah (1966) found expressions for the fundamental (F0) and first harmonic (F1) of the vibrational modes in Hertz to be

$$\mathrm{F0} = \left(\frac{4U^2}{C^2} + \frac{25\pi^2}{16}\right)^2 C/2\pi R, \tag{3}$$

and

$$\mathrm{F1} = \left(\frac{4U^2}{C^2} + \frac{81\pi^2}{16}\right)^2 C/2\pi R, \tag{4}$$

where C is the speed of sound in meters per second (a value of 330 m s^{-1} is used in making the estimates below), U is the tangential wind speed of the core, and R is the core radius. The first term in brackets involving the Mach number squared represents only a small second-order correction for core speeds below the speed of sound. In fact, for tangential wind speeds of Mach 1,

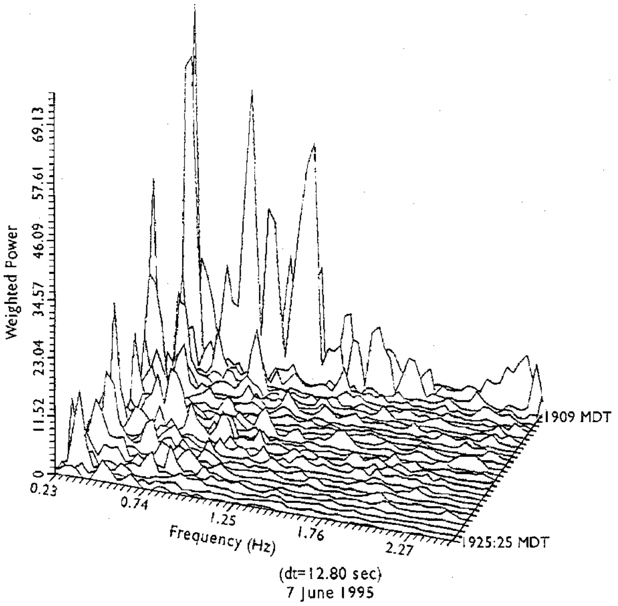

FIG. 19. Acoustic signal power as a function of frequency between 1909 and 1914 MDT. Acoustic power is proportional to the square of the measured sound pressure amplitude. Values have been weighted by multiplying by the square of the dimensionless correlation coefficient to emphasize the spectra of higher-quality signal data.

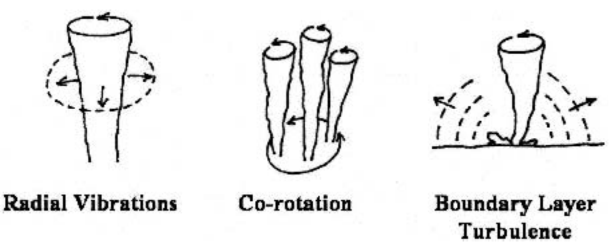

FIG. 20. Conceptual view of three vortex sound production models.

the first term in Eq. (3) is about 20% of the second term. Thus, for practical purposes, the expressions for the fundamental and first harmonic reduce to

$$\mathrm{F0} = 207/R, \tag{5}$$

and

$$\mathrm{F1} = 371/R, \tag{6}$$

where R is in meters.

The relations for the fundamental and first harmonic frequencies, F0 and F1, are plotted in Fig. 21. Two data points, together with an estimate of the range of frequencies observed, also appear on the plot at times corresponding to clearly detected tornadic rotations by the radar. The radius of the tornado was estimated from the Doppler radar measurements.

Although this case shows evidence of a sound source that was initially active aloft, which would preclude the boundary layer mechanism from explaining these measurements, it is nevertheless of interest to estimate the frequency range expected from such an acoustic generation process, which may be active under other situations. Similarly, the multiple-vortex corotation process is also of interest to evaluate.

Tatom et al. (1995) made estimates of the dominant frequencies of pressure fluctuations produced by tornadoes at the surface of the earth in order to determine the frequencies of seismic waves excited. They estimated the frequency produced as

$$F_{\mathrm{e}} = U_{\infty} k_e / 2\pi, \tag{7}$$

where U_{∞} is the wind speed, and k_e is the wavenumber of the energy-containing eddies. If x is the distance from the leading edge of the flow (using a value of one-half the radius of the vortex), and the thickness of the boundary layer between the tornado and the surface is δ, then L_e the scale of the energy-containing eddies is approximately equal to δ. Using results for the boundary layer on a rough flat surface (Blake 1970; Harrison 1967),

$$\delta/x = 0.009 = 2\delta/\mathrm{r} \quad \text{and} \quad F_{\mathrm{e}} = U_{\infty}/(0.009\,\pi r). \tag{8}$$

The boundary layer noise model cannot explain the measurements of infrasound at lower frequencies nor observations of sound from concentrated regions of rotation aloft. Nevertheless, it is an important model once strong vortex interaction with the surface has occurred and could explain the audible components from the

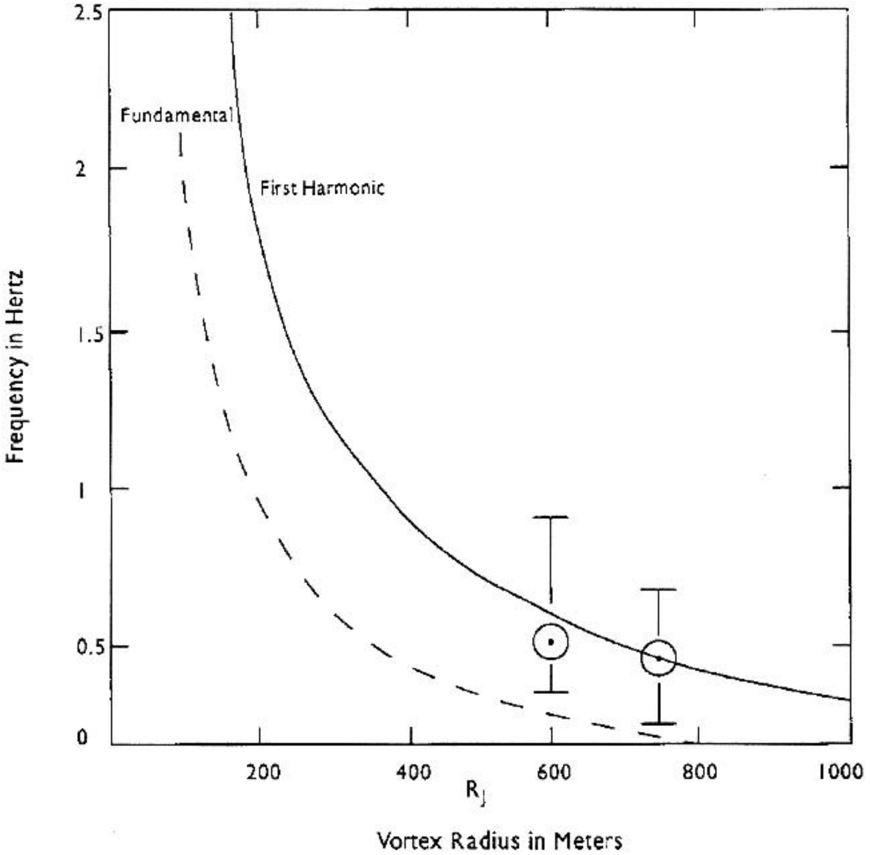

FIG. 21. Frequency of the fundamental and first harmonic of the radial modes of vibration of a vortex. Data points shown on the plot are based upon infrasonic and radar data for two times during the event. The bars refer to the measured frequency range of infrasound.

TABLE 3. The dominant predicted frequency for three acoustic source types.

Wind speed ($\mathrm{m\ s^{-1}}$)	Radius (m)	Radial modes frequency (Hz)	Tornado–surface frequency (Hz)	Corotation frequency (Hz)
50	100	2.07	18	0.2
	250	0.83	8	<0.1
	500	0.41	5	<0.1
	1000	0.2	1	<0.1
75	100	2.07	30	0.3
	250	0.83	10	<0.1
	500	0.41	7	<0.1
	1000	0.2	2	<0.1
100	100	2.07	42	0.4
	250	0.83	15	0.15
	500	0.41	10	<0.1
	1000	0.2	4	<0.1

smaller-scale populations of boundary layer eddies. This model also suggests that measurements should be made at higher infrasonic frequencies between 10 and 20 Hz. Evidence to date indicates that sound originates from the most concentrated portions of vortex columns.

Two vortices having the same circulation will rotate about a common center by mutual induction (Powell 1964; Georges 1976; Mitchell et al. 1992). The frequency of the sound emitted is twice the rotational frequency. Thus,

$$f = \omega/\pi = \Gamma/4\pi r^2 = U/\pi r, \tag{9}$$

where Γ is the circulation, U is the tangential speed of the corotation, and r is the separation radius. Assuming rotational speeds in the range of 50 to 100 $\mathrm{m\ s^{-1}}$, the system will radiate sound at frequencies between about 0.1 to 0.2 Hz.

Table 3 estimates the expected dominant frequency of these three mechanisms for a variety of conditions. The multiple-core characteristic frequency estimates were made using the assumption of two corotating vortices. This table shows that the mechanism of Abdullah (1966) produces sound in the frequency range of our observations and suggests that a limited range of frequencies will occur for a considerable range of vortex properties. Corotating vortices will tend to produce sound at significantly lower frequencies (typically, less than 0.1 Hz) than those focused on here. However, if more than two cores corotate, the frequencies produced will be higher. Note that a system of up to six vortices has been shown to be stable (Thompson 1968; Morikawa and Swenson 1971). The tornado–boundary layer interaction mechanism tends to produce sounds at higher frequencies and shows strong variability with the strength of the vortex and the core size. The nature of sounds predicted from these latter two mechanisms suggests that measurements should also be made over a broader frequency range. For the case analyzed here we cannot eliminate the possibility that these other mechanisms also produced sound outside the limits of our measurement passband.

Table 4 summarizes the frequencies predicted for various atmospheric vortices as a function of typical radii (Glickman 2000) using the radial vibration model. For the range of funnel radii, the lower limit of 50 m is based largely upon our acoustic measurements to date. In addition, aircraft wake vortices can have tangential speeds in excess of 100 $\mathrm{m\ s^{-1}}$ and concentrated cores. The predicted (and measured) frequencies for wake vortices are greater than 100 Hz, well above those of natural atmospheric vortices. Most dust devils should radiate sound above the range of tornadic sounds, while mesocyclones should produce sound below the frequencies of all but the very largest tornadoes. Thus, based upon this sound production model it is logical to define three passbands for monitoring the acoustics of intense atmospheric vortices. A passband from 1 to 5 Hz will cover most tornadoes, while a passband between 0.2 and 1 Hz will cover larger tornadoes and some mesocyclones. At higher frequencies between 5 and 10 Hz smaller tornadoes and funnels may be observed. We have detected a unique type of constant tone during some severe weather events between 5 and 10 Hz for which we have no explanation, so that there may be other interesting processes producing infrasound. Currently, our real-time processing displays data in three passbands, from 0.5 to 1 Hz, 1 to 5 Hz, and 5 to 10 Hz. Simultaneously, we have detected infrasound from different weather systems in these various frequency ranges. With postprocessing we can cover frequencies below or above these passbands and continue to evaluate optimum processing and display techniques.

6. Two significant hailstorms that did not produce infrasound

Carey and Rutledge (1998) indicate that the storm of 7 June 1995 was electrically active and produced large

TABLE 4. Characteristic frequencies of various vortices using the radial vibration model.

Vortex type	Typical radius range	Fundamental frequency (Hz)	First harmonic (Hz)
Mesocyclones	1 to 5 km	0.21 to 0.04	0.37 to 0.07
Tornadoes	100s of meters to 1 km	2.1 to 0.21	3.7 to 0.37
Funnels	50 m to 100s of meters	4.1 to 2.1	7.4 to 3.7
Dust devils	3 to >30 m	69 to 6.9	124 to 12.4
Aircraft wake vortices	1 to 2 m	207 to 104	371 to 196

hail (up to 5 cm in diameter). Although the storm was tracked from 1731 until 2028 MDT, the largest amounts of hail occurred between 1850 and 1924 MDT (the interval when we detected infrasound). But is the radiation of near infrasound a common feature of most if not all storms, resulting from a combination of processes including wind shear, electrical activity, and releases of energy by changes of state? To address this question the two hailstorms chosen for comparison were unique in that they were monitored by Doppler radar while also being studied intensively by a variety of other techniques (e.g., aircraft, mobile surface observers). One storm was documented as a CHILL radar case study and details for the other was documented by Brandes et al. (1995). The storms were significant in that they had tops extending to about 30 000 ft and produced hail with diameters greater than 2 cm. No tornadoes, funnels, or mesocyclones were reported for either of these storms, which were intensely observed.

Acoustic observatories operating for both storms (which were at ranges of less than 60 km) had low local noise levels and could have detected low-amplitude sounds had they been present. The fact that no sound was detected in the passband between 0.5 and 2.5 Hz indicates that a required acoustic generation mechanism was not present for these cases. The implication is that the presence of vortex motions may be a primary cause of severe weather infrasound near 1 Hz. These hailstorm observations are summarized in Table 5.

TABLE 5. Summary of observations of two hailstorms.

- Observatories operating near significant hailstorms with no reported funnels or tornadoes did not detect infrasound at frequencies from 0.5 to 5 Hz.
- 1809 MDT on 22 Jun 1995, CHILL radar:
  43-km range at 37°E
  3–4-cm hail
  Tops to 12 km
- 1537 MDT on 24 Jun 1992, Cloud Physics Radar (CP-2)
  60-km range at 330°E
  4.5-cm hail
  Tops to 14 km

7. Summary and conclusions

The case study of 7 June 1995 compared near-infrasonic measurements with Doppler radar tracking of the maximum circulation of a vortex as it descended from higher altitudes to the surface. The collocated infrasonic observing system followed the trend of the position of strongest rotation for about 30 min, but north of the Doppler radar bearings. Wind shear refraction could have caused the bearing offsets. Although the wind shear measured by the CHILL radar could have caused the bearing deviations, there remains the possibility that another storm feature could have radiated infrasound from another location within the storm. This observation emphasizes the need for exploring the effects of severe storm environments on measured bearings using acoustic ray trace simulations. An important note is that even with retrospective analysis of radar data, for some of the intermediate scans it was difficult to identify vortex circulations. This unique dataset permitted comparisons between the measured acoustic signatures and sound generation models. The dominant frequencies closely matched those predicted by Abdullah (1966) for the radial modes of vibration of vortices. It will also be valuable to apply fully compressible models to explore the sound generated by a variety of fluid dynamic processes. Comparative studies would be a valuable area for future collaborative research. For example, numerical model sensitivity studies could explore if and how different processes produce infrasound. The spectral content radiated by vortices of different strengths and radii could be explored.

In addition, two intensively measured, significant hailstorms with no observed vortices did not produce infrasound. This implies that vorticity in the form of mesocyclones or tornadoes may be a primary mechanism for infrasound production near 1 Hz and that other severe weather sound production mechanisms will not complicate interpretation in the 0.5- to 5-Hz passband focused on here. This point needs further examination. A review of other possible acoustic generation mechanisms suggests possibilities for monitoring a range of other aspects of storm processes and dynamics in other frequency ranges.

Key results of the study and implications for future work are outlined below:

- Frequency detected matched analytical model for radial modes of vibration of a vortex.
- Provided unique comparison between collocated infrasonic observatory and Doppler radar.
- Acoustic energy was detected earlier than the radar-velocity couplet, both originating at higher altitudes and moving to the northeast before reaching the surface. This is because the WSR-88D is constrained to operate below 20° tilt angles.
- Other possible acoustic radiation mechanisms exist that could radiate sounds higher or lower than 1 Hz.
- Infrasonic observatories could complement Doppler radars, detecting small-scale vorticity at higher altitudes and shorter ranges where radial-velocity components may be small or difficult to resolve.
- Since infrasound is detectable from long ranges (hundreds of kilometers or more), such distant identifications of well-documented, long-lived storms containing concentrated vorticity may be useful for understanding sound generation processes.

In addition, infrasonic observatories could provide the following:

- Vortex detection capabilities where radar constraints exist (e.g., obstacle blocking, longer ranges where radar resolution is degraded, short ranges where high elevation radar scans are limited).

- Detection continuity between radar scans. The interval between consecutive WSR-88D volume scans is 5 min. New volume scan strategies will soon reduce the radar scan time to about 4 min. An infrasonic observing system provides a complete scan for signals in the volume around the observatory approximately every 12 s. During 2003 infrasonic systems were located at the BAO and Weather Forecast Offices in Pueblo, Colorado, and Goodland, Kansas, presenting the 12-s locally processed data with no delay. These processed data were also brought back to Boulder, Colorado, over satellite links and land lines before being melded with radar data and placed on Web site displays for access. This process currently takes about 5 min, and we are planning to reduce this to about 1 min.
- Information on smaller diameter vortices.
- Information on vortices concentrated over limited vertical extents, which may not show clearly on volume scan displays.

The 7 June 1995 case study provided the impetus for revisiting archived infrasonic data and comparing acoustic measurements with storm data. This has resulted in the classification of over 100 cases, where infrasonic signals originated at the time of and from the direction of observed vortices. In addition, these results inspired the creation of a three-station prototype demonstration infrasonic network (ISNet), which started operation in May 2003 with increasing capabilities through the summer months. Infrasonic observatories are currently in operation at the Boulder Atmospheric Observatory; Pueblo, Colorado; and Goodland, Kansas. Analysis is in progress on the datasets created.

A key need is to insure that the infrasonic system design is optimized and covers the region or regions of the acoustic spectrum that contain important information about severe weather dynamics. A mobile infrasonic observatory, using a van capable of rapid deployment and equipped with sensors having an extended passband (0.1–200 Hz), would permit the gathering of complete "voice prints" of infrasound at relatively close ranges. It would be especially valuable operated in coordination with other systems to better document storm details. Simultaneous operation with mobile Doppler radar systems (e.g., Bluestein and Unruh 1989) would be the ideal way to expand the dataset and define the optimum passband.

Infrasonic observatories can be used in a number of ways to monitor severe weather. One valuable use when they are collocated with WSR-88D sites could be to complement the radar in identifying and tracking severe storm vorticity. Conversely, the radar data would help insure more definitive interpretations of infrasonic signals as originating from storm cells. Other sources of acoustic signals range from quite distant severe weather not affecting some local region to sounds generated by other phenomena entirely (such as turbulence aloft or large explosions). Thus, using the radar data and requiring that the acoustic azimuth coincide with a storm cell will greatly increase confidence in the interpretation of data from a single observatory.

The use of multiple regional observatories would provide the advantage of being able to triangulate and locate the origin of the sound source. In the ISNet operation, data are fed to a central point and combined with radar data for display. In the event that the signal-to-noise ratio at one observatory is reduced by high winds (e.g., from an outflow boundary), a second system could continue to provide acoustic azimuth data. Developments in noise-reducing techniques have continued to raise the wind speed threshold below which infrasound can be reliably detected. Signals have been successfully detected from the direction of mesocyclones while stations were in an outflow from a nearby thunderstorm. Further improvements in wind-noise reduction are expected.

A need exists for testing and evaluating these potential uses. Therefore, important roles exist for research Doppler radar in assessing infrasonic measurements.

Acknowledgments. The author is most grateful to a number of colleagues for making the datasets described herein possible. The impetus for the key installation at the CHILL radar site came from our collaboration with Colorado State University's Geosciences Program. Particular thanks are due R. Pielke, M. Nicholls, T. Vonder Haar, and K. Eis. For support with logistics and data at the CHILL radar site, I am grateful to S. Rutledge, P. Kennedy, and D. Brunkow. P. Kennedy was particularly helpful providing data for after-the-fact analyses. The support of W. Bach of the U.S. Army Research Office is also acknowledged. In assisting with instrumentation, both R. T. Nishiyama and S. Pezoa worked to insure that two observing systems worked reliably. A team of students assisted with installations, data archiving, preliminary analyses, collection of meteorological data, and many other tasks. These included R. Bloemker, R. Craig, L. Ferber, S. Nash, and K. Taga. Finally, I thank two anonymous reviewers for their questions, comments, and suggestions. They provided the most comprehensive and helpful reviews I have ever received.

APPENDIX

More Background Concerning Infrasonic Measurements

a. What is infrasound?

Infrasound is the range of acoustic frequencies below the audible (Bedard and Georges 2000). For a typical person this is at frequencies below about 20 Hz, where the threshold of human hearing and feeling cross over. There is a rational analog between sound and the relationship of infrared to visible light. Thus, one can call the frequency range 1 to 20 Hz near infrasound and the range from about 0.05 to 1 Hz infrasound. Below about 0.05 Hz where gravity becomes important for propagation, atmospheric waves are usually called acoustic/gravity waves. A frequency of 1 Hz is eight octaves below middle C. The lowest frequency on a piano keyboard is A at 27.5 Hz, consistent with being near the lowest limits of a typical person's hearing. Acousticians have adopted the convention of defining sound levels relative to the threshold of human hearing, and most past acoustic studies involved the perceptions of people to sound. However, the infrasonic signal data can be quite valuable and provide information on a range of geophysical processes. Infrasonic observing systems routinely need to detect sound pressure levels of 0.01 Pa (equivalent to 1 mm of pressure altitude) in the presence of noise from wind and other sources. (More background on infrasonics may be found online at http://www.etl.noaa/etl/infrasound/.)

b. What sensors and techniques are required for the detection of these low-level, low-frequency sounds? What parameters are measured?

A critical need for the measurement of infrasound was the development of an effective method for reducing noise from large but highly spatially incoherent pressure fluctuations induced by wind, while still detecting infrasonic signals. Daniels (1959) made the critical breakthrough in devising a noise-reducing line microphone. His concept was to match the impedance along a pneumatic transmission line using distributed input ports and pipe size changes to minimize attenuation. This innovation, exploiting the high spatial coherence of infrasound and the small spatial coherence of pressure changes related to turbulence, provided signal-to-noise ratio improvements of the order of 20 dB. Variations of his concept are currently in use worldwide. An infrasonic noise reducer can take the form of a spatial filter using 12 radial arms with ports at 1-ft intervals and covering a diameter of 50 ft. We have adapted porous irrigation hose for use as a distributed pressure signal transmission line (an infrasonic noise reducer), saving considerable costs in fabrication and maintenance. The present wind noise reducers can look a lot like an octopus (with four extra arms) with black porous hoses radiating outward from a central sensor.

A reasonable assumption, for sound waves from point sources after traveling paths of tens or hundreds of wavelengths, is that the wave fronts are planar. This model is usually used in processing data from infrasonic observing systems and was the basis for the design of cross-correlation algorithms developed to determine correlation coefficient, azimuth, and horizontal phase speed. Effective separations for microphones in arrays are usually about one-quarter of the primary acoustic wavelength to be detected. In addition, the fact that infrasonic signals show little change with distance is the basis of the method for the reduction of unwanted pressure noise. Figure A1 shows a typical array layout. Usually an infrasonic observatory consists of four sensors equipped with spatial filters in a rough square configuration. The 12 porous hoses are often 50 ft in length and bent back toward the center so that the complete filter covers a diameter of about 50 ft. These noise reducers can operate in rain and snow without affecting infrasonic signals. Vegetation or special barriers can reduce wind in the lower boundary layer and further improve wind-noise reduction.

Conventional microphones, designed for audio frequencies, do not respond to infrasonic frequencies. There are a number of reasons for this, in addition to the fact that there was no practical need to detect inaudible sounds. For example, extended low-frequency sensitivity could cause undesirable dynamic response limitations, because of larger pressure fluctuations at lower frequencies. Thus, a microphone having a diaphragm deflecting in response to sound waves typically has a leakage path to a reference volume behind the membrane. This permits frequencies below the cutoff of such a high-pass filter to appear on both sides of the sensor, canceling response. We use sensitive differential pressure sensors integrated with a large, well-defined reference volume and calibrated flow resistor providing a stable high-pass-filter time constant. The volume is insulated to create a stable temperature environment. These sensors are rugged, relatively small (less than 2×2×2 ft), and relatively light (about 22 lb). We typically operate continuously for years with few problems.

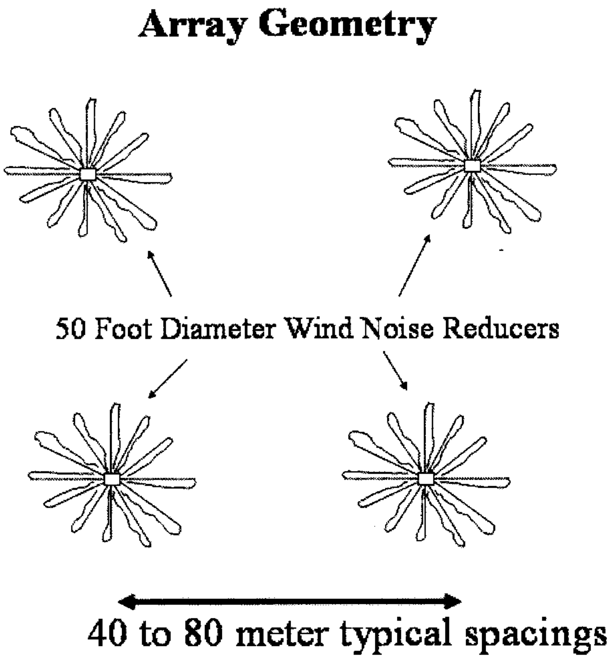
Array Geometry
50 Foot Diameter Wind Noise Reducers
40 to 80 meter typical spacings

FIG. A1. Typical layout of the four sensors of an infrasonic observatory.

TABLE A1. Parameters measured by infrasonic observatories.

Parameter	Significance
Correlation coefficient, a measure of S/N	Index of signal quality and a measure of confidence in the accuracy of other parameters
Azimuth	Critical measure of the direction from which sound is originating
Phase speed (indicating the elevation angle)	Angle of arrival can indicate the location of source regions aloft
Spectral content	The dominant frequency (frequencies) can indicate important characteristics of the sources
Sound pressure level	The amplitude, although a measure of source strength, is greatly affected by propagation
Duration	Typical vortex-related signals continue for tens of minutes or more. Signals of very short durations (e.g., ~1 min) are unlikely to be related to a coherent vortex.
Persistence	Even at low S/Ns, confidence can be obtained in the characterization of signal sources if they persist for significant periods of time. Histograms of parameters over interval can quantify distributions and, e.g., identify source direction even for weak signals

Because arrays of sensors are applied to detect and process signals, there is a need to match the microphone sensitivities and phase characteristics. This required the creation of a family of static and dynamic pressure calibration techniques, as well as methods for measuring flow resistance. The infrasonic sensors are carefully matched and interchangeable. The current cost of an infrasonic observatory (including processing and display hardware) is about $50,000. Wilczak and Bedard (2004) provide further details concerning sensor design.

The parameters measured by an infrasonic observing system are summarized in Table A1, which includes comments about their practical significance for monitoring vortices. A variety of alternative processing techniques continue to be evaluated. Unlike the detection of earthquakes, where single seismometers often provide effective detection, infrasonic geophysical measurements require arrays of sensors at each observing site because of the complex signal and noise environments encountered. Infrasonic observatories have detected sound from a wide variety of phenomena. The sources measured range from transient luminescent events (TLEs; e.g., sprites, blue jets) to earthquakes. Our experience to date is that these will not represent significant false alarms for tornado detection applications.

REFERENCES

Abdullah, A. J., 1966: The “musical” sound emitted by a tornado. *Mon. Wea. Rev.,* **94,** 213–220.

Anderson, F. J., and G. D. Freier, 1965: The role of wave motion in a tornado. *J. Geophys. Res.,* **70,** 2781–2784.

Arnold, R. T., H. E. Bass, and L. N. Bolen, 1976: Acoustic spectral analysis of three tornadoes. *J. Acoust. Soc. Amer.,* **60,** 584–593.

Balachandran, N. K., 1979: Infrasonic signals from thunder. *J. Geophys. Res.,* **84,** 1735–1745.

Bass, H. E., 1980: The propagation of thunder through the atmosphere. *J. Acoust. Soc. Amer.,* **67,** 1959–1966.

Beasley, W. H., T. M. Georges, and M. W. Evans, 1976: Infrasound from convective storms: An experimental test of electrical source mechanisms. *J. Geophys. Res.,* **81,** 3133–3140.

Bedard, A. J., Jr., 1971: Seismic response of infrasonic microphones. *J. Res. Natl. Bur. Stand.,* **75C,** 41–45.

——, 1977: The D-C pressure summator: Theoretical operation, experimental tests, and possible practical uses. *Fluid. Quart.,* **9,** 26–51.

——, 1988: Infrasound from natural sources. *Proc. Inter-Noise ’88,* Avignon, France, Société Française d’Acoustique, 927–930.

——, 1994: Evaluation of atmospheric infrasound for monitoring avalanches. *Proc. Seventh Int. Symp. on Acoustic Remote Sensing and Associated Techniques of the Atmosphere and Oceans,* Boulder, CO, NOAA/ERL/Environmental Technology Laboratory, 5-13–5-22.

——, 1998: Infrasonic detection of severe weather. Preprints, *19th Conf. on Severe Local Storms,* Minneapolis, MN, Amer. Meteor. Soc., 218–219.

——, and G. E. Greene, 1981: A case study using arrays of infrasonic microphones to detect and locate meteors and meteorites. *J. Acoust. Soc. Amer.,* **65,** 1277–1279.

——, and T. M. Georges, 2000: Atmospheric infrasound. *Phys. Today,* **53,** 32–37.

——, J. Intrieri, and G. E. Greene, 1986: Infrasound originating from regions of severe weather. *Proc., 12th Int. Congress on Acoustics,* Toronto, ON, Canada, J2–5.

——, G. E. Greene, J. Intrieri, and R. Rodriguez, 1988: On the feasibility of detecting and characterizing avalanches by monitoring radiated subaudible atmospheric sound at long distances. *Proc. Conf. on a Multidisciplinary Approach to Snow Engineering.* Santa Barbara, CA, U.S. Army Corps of Engineers, Cold Regions Research and Engineering Laboratory, 267–275.

——, R. W. Whitaker, G. E. Greene, P. Mutschlecner, R. T. Nishiyama, and M. Davidson, 1992: Measurements of pressure fluctuations near the surface of the earth. Preprints, *10th Symp. on Turbulence and Diffusion,* Portland, OR, Amer. Meteor. Soc., 293–296.

Blake, W. K., 1970: Turbulent boundary-layer wall-pressure fluctuations on smooth and rough walls. *J. Fluid Mech.,* **44,** 637–660.

Bluestein, H. B., and W. P. Unruh, 1989: Observations of the wind field in tornadoes, funnel clouds, and wall clouds with a portable Doppler radar. *Bull. Amer. Meteor. Soc.,* **70,** 1514–1525.

Bohannon, J. L., A. A. Few, and A. J. Dessler, 1977: Detection of infrasonic pulses from thunderclouds. *Geophys. Res. Lett.,* **4,** 49–52.

Bowman, H. S., and A. J. Bedard Jr., 1971: Observations of infrasound and subsonic disturbances related to severe weather. *Geophys. J. Roy. Astron. Soc.,* **26,** 215–242.

Brandes, E. A., J. Vivekanandan, J. D. Tuttle, and C. J. Kessinger, 1995: A study of thunderstorm microphysics with multiparameter radar and aircraft observations. *Mon. Wea. Rev.,* **123,** 3129–3143.

Brooks, E. M., 1951: Tornadoes and related phenomena. *Compendium of Meteorology,* T. Malone, Ed., Amer. Meteor. Soc., 673–680.

Carey, L. D., and S. A. Rutledge, 1998: Electrical and multiparameter radar observations of a severe thunderstorm. *J. Geophys. Res.,* **103** (D12), 13 979–14 000.

Colgate, S. A., and C. McKee, 1969: Electrostatic sound in clouds and lightning. *J. Geophys. Res.,* **74,** 5379–5389.

Cook, R. K., 1962: Strange sounds in the atmosphere, Part 1. *Sound,* **1,** 12–16.

——, and A. J. Bedard Jr., 1971: On the measurement of infrasound. *Geophys. J. Roy. Astron. Soc.,* **26,** 5–11.

Daniels, F. B., 1959: Noise reducing line microphone for frequencies below 1 cps. *J. Acoust. Soc. Amer.,* **31,** 529–531.

Depasse, P., 1994: Lightning acoustic signatures. *J. Geophys. Res.,* **99,** 25 933–25 940.

Dessler, A. J., 1973: Infrasonic thunder. *J. Geophys. Res.,* **78,** 1889–1896.

Einaudi, F., A. J. Bedard Jr., and J. J. Finnigan, 1989: A climatology of gravity waves and other coherent disturbances at the Boulder Atmospheric Observatory during March–April 1984. *J. Atmos. Sci.,* **46,** 303–329.

Few, A. A., 1979: Acoustic radiation from lightning. *CRC Handbook of Atmospherics,* Vol. II, H. Volland, Ed., CRC Press, 257–290.

Georges, T. M., 1972: Acoustic ray paths through a model vortex with a viscous core. *J. Acoust. Soc. Amer.,* **51,** 206–209.

——, 1973: Infrasound from convective storms: Examining the evidence. *Rev. Geophys. Space Phys.,* **11,** 571–593.

——, 1976: Infrasound from convective storms. Part II: A critique of source candidates. NOAA Tech. Rep. ERL 380–WPL 49, 59 pp. [Available from the National Technical Information Service, 5285 Port Royal Rd., Springfield, VA 22161.]

——, and G. E. Greene, 1975: Infrasound from convective storms. Part IV: Is it useful for warning? *J. Appl. Meteor.,* **14,** 1303–1316.

——, and W. H. Beasley, 1977: Infrasound refraction by winds. *J. Acoust. Soc. Amer.,* **61,** 28–34.

Glickman, T. S., 2000: *Glossary of Meteorology.* 2d ed. Amer. Meteor. Soc., 855 pp.

Gossard, E. E., and W. H. Hooke, 1975: *Waves in the Atmosphere: Atmospheric Infrasound and Gravity Waves—Their Generation and Propagation.* Elsevier Scientific, 456 pp.

Harrison, A. J. M., 1967: Boundary layer displacement thickness on flat plates. *J. Hydraul. Div. Amer. Soc. Civ. Eng.,* **93,** 79–91.

Hazen, H. A., 1890: Tornado losses and insurance. *Science,* **16,** 15–19.

Hicks, W. M., 1884: On the steady motion and the small vibrations of a hollow vortex. *Philos. Trans. Roy. Soc. London,* **175,** 161–195.

Hubbert, J., V. N. Bringi, L. D. Cary, and S. Bolen, 1998: CSU–CHILL polarimetric radar measurements from a severe hailstorm in eastern Colorado. *J. Appl. Meteor.,* **37,** 749–775.

Jones, R. M., and T. M. Georges, 1976: Infrasound from convective storms. III. Propagation to the ionosphere. *J. Acoust. Soc. Amer.,* **59,** 765–779.

Kozel, V., G. H. Vatistas, and J. Wang, 1992: The influence of internal waves on the structure of vortex cores. *Proc. 30th Aerospace Sciences Conf.,* Reno, NV, American Institute of Aeronautics and Astronautics, Paper AIAA 92–0058, 7 pp.

Lamb, H., 1945: *Hydrodynamics.* Dover, 738 pp.

Lyamshev, L. M., and A. T. Skvortsov, 1988: Sound radiation by localized vortices in a slightly compressible medium (Review). *Sov. Phys. Acoust.,* **34,** 447–459.

Meecham, W. C., 1971: On aerodynamic infrasound. *J. Atmos. Terr. Phys.,* **33,** 149–155.

Mitchell, B. E., S. K. Lele, and P. Moin, 1992: Direct computation of the sound from a compressible corotating vortex pair. *Proc. 30th Aerospace Sciences Conf.,* Reno, NV, American Institute of Aeronautics and Astronautics, Paper AIAA 92–0374, 9 pp.

Morikawa, G. K., and E. V. Swenson, 1971: Interacting motion of rectilinear geostrophic vortices. *Phys. Fluids,* **14,** 1058–1073.

Nicholls, M. E., R. A. Pielke, and W. R. Cotton, 1991: Thermally forced gravity waves in an atmosphere at rest. *J. Atmos. Sci.,* **48,** 1869–1884.

Pielke, R. A., M. E. Nicholls, and A. J. Bedard Jr., 1993: Use of thermal compression waves to assess latent heating from clouds. *Eos, Trans. Amer. Geophys. Union,* **74,** 493.

Powell, A., 1964: Theory of vortex sound. *J. Acoust. Soc. Amer.,* **36,** 177–195.

Tatom, F. B., K. R. Knupp, and S. J. Vitton, 1995: Tornado detection based on seismic signal. *J. Appl. Meteor.,* **34,** 572–582.

Thompson, J. J., 1968: *A Treatise on the Motion of Vortex Rings.* Dawsons of Pall Mall, 124 pp.

Thompson, W., 1910: Vibrations of a columnar vortex. *Hydrodynamics and General Dynamics,* J. Larmor, Ed., Mathematical and Physical Papers, Vol. IV, Cambridge University Press, 152–165.

Wilczak, J. M., and A. J. Bedard Jr., 2004: A new turbulence microbarometer and its evaluation using the budget of horizontal heat flux. *J. Atmos. Oceanic Technol.,* **21,** 1170–1181.